# Physical−Chemical Characterization of Binary Mixtures of 1-Butyl-1-methylpyrrolidinium Bis{(trifluoromethyl)sulfonyl}imide and Aliphatic Nitrile Solvents as Potential Electrolytes for Electrochemical Energy Storage Applications

Alex R. Neale,[*,†] Christoph Schütter,[‡,§,∥] Patrick Wilde,[†] Peter Goodrich,[†] Christopher Hardacre,[†,#] Stefano Passerini,[‡,§] Andrea Balducci,[‡,§,∥] and Johan Jacquemin[*,†,Ω]

[†]School of Chemistry and Chemical Engineering, David Keir Building, Queen's University Belfast, Belfast, Northern Ireland BT9 5AG, United Kingdom

[‡]Helmholtz Institute Ulm, Helmholtzstraße 11, 89081 Ulm, Germany

[§]Karlsruhe Institute of Technology (KIT), PO Box 3640, 76021 Eggenstein-Leopoldshafen, Germany

**S** *Supporting Information*

**ABSTRACT:** In the scope of improving the energy and power densities of electrochemical double layer capacitors (EDLCs), the development of high performance electrolytes with enhanced operative voltages is imperative. The formulation of mixtures containing ionic liquids with organic molecular solvents is an important strategy in the pursuit of developing highly electrochemically stable and safe materials while retaining fast transport properties for high power applications. In this work, we report on the physical−chemical investigations into binary mixtures containing the ionic liquid 1-butyl-1-methylpyrrolidinium bis{(trifluoromethyl)sulfonyl}imide with one mononitrile solvent, butyronitrile, and two dinitrile solvents, glutaronitrile and adiponitrile, as potential electrolytes for EDLCs. The thermal, volumetric, and transport properties of the binary mixtures are investigated as functions of the electrolyte composition and temperature. Furthermore, the electrolyte composition which exhibits the highest conductivity for each of the binary mixtures was determined, and its electrochemical stability is reported using a glassy carbon macrodisk electrode.
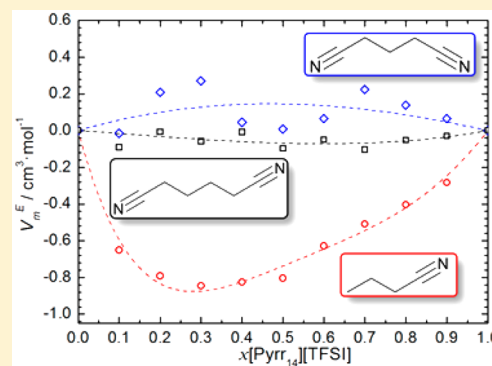
## 1. INTRODUCTION

The drive to develop high capacity and high power electrical energy storage devices is a key factor for the practical realization of alternative renewable energy sources which are inherently intermittent in nature. Of the range of developing energy storage systems, including batteries and fuel cells, electrochemical double layer capacitors (EDLCs) appear as one of the most promising technologies, particularly for high-power applications. The mechanism of energy storage in EDLCs is based on physical processes wherein electrostatic charge separation occurs at an electrode/electrolyte interface in response to applied electrode potentials. Since the processes during charge/discharge cycling of an EDLC are purely physical, unlike in batteries which rely on reversible redox electron transfer reactions, high currents can be utilized to achieve complete charge/discharge in seconds (i.e., high power outputs) through hundreds of thousands of cycles without significant capacity fade.[1−3] Nevertheless, the nature of the charge/discharge processes ensure that, relative to conventional Li-ion batteries, the total energy density of EDLCs is significantly low, typically less than 6 Wh·kg$^{-1}$.[3] Consequently,

the focus of most of the work surrounding EDLCs lies with increasing the energy density by means of developing novel high-capacity electrode materials, such as templated carbide-derived carbons,[4,5] and graphene-derived carbons,[6,7] as well as, by the formulation of new and more stable electrolytes which may afford enhanced operative voltages.[8−14]

The capability of a particular electrolyte to promote the performance of an EDLC can be partially understood by the following relationships between the specific energy, $E = 0.5CV^2$, and the specific power, $P = V^2/(4R)$, of an EDLC and the operative voltage, $V$, of the device (where $R$ and $C$ represent the internal resistance and the capacitance of the EDLC, respectively). Given these dependencies, it can be seen that even small increases in the operative voltage of the EDLC could lead to significant improvements in the achievable energy density of an EDLC device. Furthermore, reducing electrolyte contributions to the internal resistance by utilizing high-

conductivity and low viscosity electrolyte formulations is important in the fabrication of high-power devices.

At present, the conventional electrolyte formulations for nonaqueous EDLCs are based on either acetonitrile (ACN) or propylene carbonate (PC) as the solvent with tetraethylammonium tetrafluoroborate ($[Et_4N][BF_4]$) as the electrolyte salt. As such, EDLCs with these electrolyte formulations can typically be utilized with an operative voltage between 2.5 and 2.8 V.[3,15] These electrolyte formulations have been studied in-depth and are continually optimized for EDLC application and, as such, can deliver high performances over hundreds of thousands of cycles.[1] However, the inherent volatility and flammability of the solvents, particularly ACN, creates potential safety issues for EDLC application. Additionally, the solubility of traditional EDLC salts in these solvents imposes limitations on the maximum achievable performance of these electrolyte formulations and it has been shown that higher electrolytic conductivities can be achieved using higher concentrations of alternative salts (e.g., 1-ethyl-3-methylimidazolium tetrafluoroborate, $[EMIm][BF_4]$).[3,16] Furthermore, higher concentrations of a nonvolatile ionic component within the electrolyte solution may be utilized to effectively reduce the vapor pressure of the resulting formulation and help to negate the potential flammability of the electrolytes.[17] Such considerations are of paramount importance for the development of safer electrolytes for EDLCs and electrochemical energy storage devices, in general.

In this particular context, ionic liquids (ILs) typically possess many inherent chemical-physical properties, notably their nonvolatility and good (electro)chemical and thermal stability, which make these liquids attractive potential candidate materials for the development of safer EDLCs,[8,13,18,19] and other electrochemical devices such as lithium-ion,[20−22] and sodium-ion secondary batteries.[23,24] Because of the purely ionic nature, and intrinsic conductivity, of ILs, several recent studies have detailed the use of neat ILs as solvent-free electrolyte systems in EDLCs. For example, operative voltages of up to 3.7 V were achieved using well-studied ILs, for example, 1-butyl-1-methylpyrrolidinium bis{(trifluoromethyl)sulfonyl}imide, $[Pyrr_{14}][TFSI]$.[8,13,25] Nevertheless, at ambient temperatures, ILs typically exhibit much higher viscosities than traditional organic solvents and, as such, the associated conductivity of the electrolyte is low and the mobility of the ionic species is sluggish. These properties, in turn, ultimately limit the power outputs of EDLC devices based on a solvent-free IL electrolyte. In this respect, two primary strategies are reported by researchers in this field. First, the design and testing of novel IL structures with effectively reduced viscosity and improved transport properties; for example, ILs containing a pyrrolidinium-based cation (with alkyl or alkoxy-group functionality) paired with the dicyanamide, $[N(CN)_2]^-$, anion have been reported to exhibit greatly improved conductivities and rate capabilities in EDLCs relative to their $[TFSI]^-$ anion-based analogues.[18] Second, investigations into the performance of blended electrolytes whereby the traditional salt ($[Et_4N][BF_4]$) is replaced with an IL and mixed with a solvent have demonstrated the possibility of synergistic improvements and significantly improved transport properties. Notably, some examples of these solvents include, for example, the conventional EDLC solvents, ACN and PC,[3,12,25−27] or alternative solvents, including adiponitrile,[11,14] or other mononitrile solvents,[9] with more desirable properties (e.g., wider electrochemical windows or low volatility).

As indicated, ILs may typically be utilized in greater concentrations within a solvent owing to the typical mutual solubility of the selected ILs with organic nitrile and carbonate solvents. As such, higher conductivities may be achieved at higher concentrations of certain IL salts and, due to the ionic nature of these liquids, increasing the IL concentration to IL-rich formulations would effectively lower the vapor pressure (Raoult's Law) and improve the safety of the electrolyte mixture.

In this study, we report on the chemical−physical characterization of a series of binary mixtures between an IL and a series of aliphatic nitrile solvents. The mononitrile solvent, butyronitrile, and the two dinitrile solvents, glutaronitrile and adiponitrile, form the solvent component of the three reported binary mixtures while $[Pyrr_{14}][TFSI]$ is utilized as the IL component. Thermal and physical−chemical characterization is reported as a function of the electrolyte composition to investigate effects of solvent−structure and IL quantity on the important features of the electrolyte compositions for EDLC application. Furthermore, investigations of the performance of a selection of these binary mixtures as EDLC electrolytes was recently reported elsewhere.[28]

## 2. EXPERIMENTAL PROCEDURES

**2.1. Materials.** Butyronitrile (BTN, ≥ 99%), glutaronitrile (GLN, 99%), adiponitrile (ADN, 99%), N-methylpyrrolidine (99%), 1-bromobutane (98%), and ferrocene (98%) were purchased from Sigma-Aldrich. Lithium bis{(trifluoromethyl)sulfonyl}imide (battery grade) was purchased from 3M. All materials were used as received. To avoid further contamination with moisture from the atmosphere, the nitrile solvents were stored in a glovebox under an argon atmosphere with a moisture content below 3 ppm.

**2.2. Synthesis of 1-Butyl-1-methylpyrrolidinium Bis-{(trifluoromethyl)sulfonyl}imide, $[Pyrr_{14}][TFSI]$.** Under an inert atmosphere, 1-bromobutane (27.4 g, 0.2 mol) was added dropwise to a solution of N-methylpyrrolidine (17.01 g, 0.2 mol) in acetonitrile (50 cm³) while the solution was stirred and cooled under an ice−water bath. The resulting mixture was allowed to warm to room temperature and was stirred vigorously overnight under reflux conditions. Volatiles were removed to leave a yellowish solid product. The solid was washed with a mixture of acetone and diethyl ether and a white solid product (43.48 g, 98%) was obtained after filtration and drying. This product, 1-butyl-1-methylpyrrolidinium bromide ($[Pyrr_{14}]Br$), was characterized using $^1H$ NMR spectroscopy: (300 MHz, DMSO) δ: 3.50 (m, 4H), 3.38 (m, 2H), 3.02(s, 3H), 2.08 (s, 4H), 1.68 (m, 2H), 1.31(m, 2H), 0.92(t, J = 7.1 Hz, 3H).

A solution of the halide salt, $[Pyrr_{14}]Br$, (0.05 mol) in dichloromethane (50 cm³) was combined with a solution of lithium bis{(trifluoromethyl)sulfonyl}imide (15.2 g, 0.053 mol) in distilled water (50 cm³) in a 250 cm³ round-bottom flask. The mixture was left to stir vigorously at room temperature overnight. The two phases were then separated using a separating funnel and the organic phase containing the ionic liquid, $[Pyrr_{14}][TFSI]$ (20.5 g, 98%), was washed several times with distilled water (10 × 10 cm³). The ionic liquid was then partially dried in vacuo (333.15 K, 0.02 mbar) and then characterized by $^1H$ and $^{13}C$ NMR spectroscopy at 293.15 K on a Bruker Avance DPX spectrometer at 300 and 75 MHz, respectively. Lithium content was analyzed by inductively coupled plasma optical emission spectroscopy (ICP-OES) on

an Agilent 5100 ICP-OES and in combination CHNS microanalysis was performed by Analytical Services at Queen's University Belfast:

$^1$H NMR (300 MHz, DMSO) $\delta$: 3.62 (m, 4H), 3.40 (m, 2H), 3.13 (s, 3H), 1.78 (d, 4H), 1.54 (m, 4H), 1.34 (m, 2H), 0.91 (t, 3H). $^{13}$C NMR (75 MHz, DMSO) $\delta$: 126.26 (s), 122.00 (s), 117.73 (s), 113.46 (s), 63.78 (s), 63.28 (s), 47.85 (s), 40.46 (t, $J$ = 19.3 Hz), 40.17 (s), 40.12−40.05 (m), 39.77 (d, $J$ = 18.8 Hz), 39.65 (s), 39.48 (d, $J$ = 20.9 Hz), 39.06 (s), 25.29 (s), 21.43 (s), 19.67 (s), 13.81 (s). CHNS theoretical: C, 31.28; H, 4.77; N, 6.63; S, 15.18. Found: C, 31.69; H, 5.15; N, 6.28; S, 15.01. Li content 23 ppm.

**2.3. Sample Preparation and Physical Measurements.** Prior to any measurements, the IL was dried under vacuum (ca. $10^{-3}$ mbar) at elevated temperature (383.15 K) with continuous stirring for a minimum of 2 days. After this procedure, the IL was stored in the Ar-filled glovebox (<3 ppm of $H_2O$) to limit water contamination. The water content of the IL and the three nitrile molecular solvents was analyzed by Karl Fischer Coulometric titration using an 899 Coulometer (Metrohm). Measurements of water content were completed in duplicate and the resolution of the measurements was 0.001 wt % or 10 ppm.

The electrolyte blends were prepared by mass, under the Ar atmosphere of the glovebox, using a Sartorius BP 110 S scale ($\pm$0.1 mg) at a temperature of ca. 305.15 K. For all reported blend formulations, both liquids were completely miscible and complete mixing was easily achieved. For each of the nitrile solvents, 11 binary electrolyte blends were prepared from $x_{IL}$ = 0 to $x_{IL}$ = 1, in increments of 0.1, with the generic formula $(x)[Pyrr_{14}][TFSI] - (1-x)nitrile$ (where *nitrile* refers to either BTN, GLN or ADN). The electrolyte blends were prepared within an accuracy of $\pm$0.0002 with respect to the molar fraction of IL, $x_{IL}$ or $x[Pyrr_{14}][TFSI]$ and an average deviation of $\pm$0.0003 from the target formulation. Once prepared, electrolyte blends were stored under the argon atmosphere and experimental analysis was completed within 2 days of the preparation. This factor was particularly important for the blends containing BTN; evaporation of the more volatile mononitrile solvent from the binary mixture over time was found to have a significant effect on the subsequently measured properties.

Density measurements were performed using a DM40 (Mettler Toledo, $\pm 1 \times 10^{-4}$ g·cm$^{-3}$) oscillating tube density meter in the range of (293.15−333.15) K ($\pm$0.01 K). Prior to any measurements, the instrument was cleaned with acetone and dried with dehumidified air. Calibration of the density meter was completed using distilled water and dehumidified air. The viscosity of the mixtures was measured using an AMVn (Anton Paar) falling/rolling ball viscometer with a 1.8 mm nominal diameter capillary (2.5−70 mPa·s range, $\pm$1% repeatability, $\pm$3% uncertainty) in the range of (293.15−333.15) K ($\pm$0.01 K) at atmospheric pressure. The capillary was calibrated using appropriate viscosity standards (Paragon Scientific Ltd.) and, for each mixture, the viscosity was taken as an average of six measurements per temperature step giving a typical average absolute deviation of less than 2% around the mean. Thermal phase transitions were recorded using differential scanning calorimetry (DSC) traces on a DSC Q2000 (TA Instruments) collected using 5 K·min$^{-1}$ heating rates (183.15 K and 323.15/333.15 K ($\pm$0.1 K) were used as the lower and upper temperature limits, respectively). Hermetically
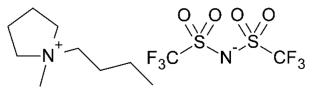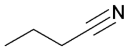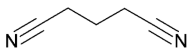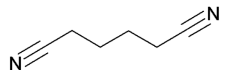
sealed Al pans containing the respective liquid sample were prepared inside the Ar-filled glovebox for DSC analysis.

Conductivity measurements were performed using a sensION+ EC71 benchtop meter with a 3-pole platinum sensION+ 5070 conductivity probe (<0.5% of range) with an in-built Pt1000 temperature probe (Hach Lange). The conductivity probe was calibrated using aqueous KCl standard conductivity solutions (147 $\mu$S·cm$^{-1}$, 1413 $\mu$S·cm$^{-1}$, and 12.88 mS·cm$^{-1}$ at 298 K). Measurements of the conductivity as a function of the formulation were completed inside the Ar-filled glovebox at 305 $\pm$ 1 K (as dictated by the internal atmosphere of the glovebox). For these measurements, a fixed mass of one component was accurately weighed into a custom-built two-necked glass flask with a small stirrer bar, and the conductivity probe was inserted into the liquid sample via one neck. The conductivity and temperature of the pure component were then recorded. Small amounts of the second component were then added to the liquid via the second neck on the flask, and the mass of each addition was accurately recorded. The solution was then mixed well to ensure homogeneity, and the conductivity and temperature of the liquid solution were recorded after a stable reading was observed. This process of adding a small amount of the second component, followed by mixing and measuring the resulting conductivity was continued to give a wide range compositions of the binary mixtures. Measurements of the conductivity as a function of temperature were prepared inside an Ar-filled glovebox by immersion of the probe in the liquid sample in a glass tube and then sealed using an O-ring seal and Parafilm. The conductivity of the sample was then measured as a function of temperature within the range of (293−363) K ($\pm$0.2 K). The temperature of the sample was varied using a small oil bath and the temperature and conductivity of the sample was recorded when the values were stable for ca. 1 min.

Measurements of the electrochemical stability window of the electrolytes by cyclic voltammetry were performed using either an Autolab PGSTAT302 workstation (Metrohm) or a VMP3 workstation (BioLogic). Measurements were performed inside an Ar-filled glovebox with moisture levels less than 3 ppm water using a three-electrode glass cell. The working electrode was a glassy-carbon macro-disk (ALS Co., Ltd., 3 mm diameter). Prior to all experiments, the glassy carbon working electrode was polished using alumina slurries of decreasing grain size (1.0 $\mu$m, 0.3 $\mu$m, and 0.05 $\mu$m) in distilled water. The electrode was then sonicated in methanol or acetonitrile and separately in distilled water for 2−3 min per solvent then dried at ca. 373.15 K in an oven. The counter electrode was platinum-coiled wire heat-sealed in a glass capillary. The Ag[NO$_3$]/Ag reference electrode consisted of silver wire immersed in a 0.1 mol·dm$^{-3}$ solution of Ag[NO$_3$] in 1-butyl-3-methylimidazolium nitrate ([BMIm][NO$_3$]) separated from the bulk solution by a glass-frit tip. The reference potential of the Ag[NO$_3$]/Ag electrode was referenced versus an internal ferrocene couple; after completion of the electrochemical window, a small quantity of ferrocene was dissolved in the liquid sample and cyclic voltammetry was used to determine the redox potentials of reversible ferrocene oxidation ($E_{Fc+/Fc}$ = +0.16 V vs the Ag[NO$_3$]/Ag reference electrode).

During standard cyclic voltammetry experiments, performed to determine the electrochemical window of each electrolyte solution, the potential of the working electrode was cycled at 2 mV·s$^{-1}$ between −5 V and +5 V versus Ag[NO$_3$]/Ag. For this study, the onset potential of electrochemical oxidative or

378

**Table 1. Names, Sources, Chemical Structures, Purity, Analysis Methods and Water Content of the Materials Used in this Investigation**

| Component | Source | Structure | Purity / mole fraction | Analysis method | $H_2O$ / ppm |
|---|---|---|---|---|---|
| $[Pyrr_{14}][TFSI]$ | Synthesis | | > 0.99 | CHNS; NMR; KF; ICP. | < 150 |
| BTN | Sigma Aldrich | | ≥ 0.99 | Stated by supplier | < 570 |
| GLN | Sigma Aldrich | | 0.99 | Stated by supplier | < 290 |
| ADN | Sigma Aldrich | | 0.99 | Stated by supplier | < 250 |

reductive bulk decomposition of the electrolyte was defined as the potential at which a current of $\pm 0.1$ mA·cm$^{-2}$ was recorded; $\pm 0.5$ mA·cm$^{-2}$ was selected as an appropriate current boundary for cycling since it is sufficiently high to indicate the onset for electrolyte decomposition, but it is not too high to excessively decompose the IL before the potential is cycled in the opposite direction. All the electrochemical measurements were conducted at a temperature of $305 \pm 1$ K as dictated by the internal atmosphere of the Ar-filled glovebox.

## 3. RESULTS AND DISCUSSION

The structure of the IL and the nitrile-based solvents are presented in Table 1 along with the purity and water level in each component. The $^1$H NMR spectrum of the reaction intermediate, $[Pyrr_{14}]Br$, and the $^1$H and $^{13}$C NMR spectra of the as synthesized $[Pyrr_{14}][TFSI]$ are presented in Figures S1 to S3, respectively, in the Supporting Information. $[Pyrr_{14}]$-$[TFSI]$ is a very commonly used, and well understood, IL and has been reported as an electrolyte component for EDLCs in several publications owing to its reasonable viscosity and high operating voltage.[8,13,26] The nitrile-based solvents selected include the mononitrile, BTN, and the two dinitrile solvents, GLN and ADN. The mononitrile solvent provides an alternative, longer alkyl chain comparison with acetonitrile; the solvent most commonly used in commercial EDLCs. The dinitrile solvents were selected because of recent reports which provide evidence that this class of solvents should exhibit good electrochemical stability and drastically lower the volatility of the solvent mixture relative to analogous acetonitrile-based electrolytes.[11,14,29]

**3.1. Thermal Properties.** The thermal phase transitions of the binary mixtures containing BTN and ADN were studied using DSC, as described in the experimental section, as a function of the composition. The temperature was scanned at 5 K·min$^{-1}$ from room temperature to 183.15 K and held at this temperature for 5 min; the sample was then scanned to 323.15 or 333.15 K and held at this temperature for 5 min and then returned to room temperature. This experiment was repeated through 2/3 cycles and the resulting collections of DSC traces for the BTN and ADN mixtures are presented in Figure S4 and Figure S5, respectively. Endothermic and exothermic peaks, with a standard uncertainty of approximately $\pm 1$ K, are given the arbitrary labels $T_f$ and $T_{cc}$ or $T_m$, respectively. The DSC trace observed for the neat IL, $x_{IL} = 1$ (Figure S4a and Figure S5a), is in good agreement with previously reported examples where fast cooling/heating rates are used.[30−33] No phase transitions were observed on cooling but, during heating, a sharp exothermic crystallization peak ($T_f = 219$ K) is observed

before two sequential endothermic peaks are observed. These two endothermic peaks are associated with a solid−solid phase transformation ($T_{cc} = 244$ K) and the melting of the IL ($T_m = 253$ K). Where peak values for phase transitions are given for $T_f$, $T_{cc}$ and $T_m$ in previous literature utilizing faster heating/cooling rates, good agreement in the observed phase transitions (i.e., within several degrees Kelvin) is observed for some examples ($[T_{cc} = 249$ K and $T_m = 255$ K],[32] $[T_f = 220$ K, $T_{cc} = 243$ K and $T_m = 255$ K][33]) but deviations are larger with others ($[T_m = 260$ K],[31] $[T_f = 210$ K, and $T_m \approx 265$ K][34]). The origin of these deviations will, of course, be effected by chemical impurities in any of the studied samples but, as some of the cited articles discuss, will be the effect of experimental conditions (i.e., heating/cooling rates). In addition to the obvious phase transitions observed in Figures S4 and S5, when this particular IL is quickly cooled and no freezing transition is observed, the IL is expected to undergo supercooling into the glassy state. As such, when the sample is then heated a glass transition may be observed. Glass transitions have been observed for this IL to be in the region of (186 to 192) K.[31,32,35] The inset graph in Figure S4a shows some evidence of a small endothermic process occurring within the region of (186 to 189) K but due to its positioning very close to the switching temperature and the small magnitude of the response, it cannot be accurately assigned as a peak.

For the BTN-containing mixtures (Figure S4), no features are observed in the DSC measurements of solvent-rich mixtures where $x_{IL} \leq 0.5$. For the pure solvent, $x_{IL} = 0$, no features are observed in the DSC traces. This is not a surprise since the reported melting point of BTN, ca. 160 K, lies well outside the studied temperature range.[36]

The lack of any features in the solvent-rich binary mixtures shows a wider low-temperature liquid range relative to the pure IL. For the IL-rich mixtures, from $x_{IL} = 0.9$ to 0.6, further addition of BTN results in gradual suppression of the thermal phase changes observed in neat IL (Figure S4a). For example, the crystallization transition, $T_f$, observed during heating at ca. 219 K in the neat IL decreases in temperature (and peak size) upon addition of BTN. Different behavior was observed for the ADN-containing mixtures, shown in Figure S5. The reported melting temperature of the pure dinitrile solvent is ca. 273.2 K.[11] A large significant exothermic peak is observed at ca. 247 K for the DSC of the pure solvent (Figure S5j) which would be associated with the delayed onset of crystallization of the liquid. With further addition of the IL, this position of this peak is reduced and the magnitude is suppressed. The DSC traces of the solvent-rich compositions show similar behavior in comparison to binary mixtures containing ADN and 1-ethyl-

1-methylimidazolium bis{(trifluoromethyl)sulfonyl}imide, [EMIm][TFSI], reported previously.[11] As observed in the BTN mixtures, addition of the solvent to the neat IL results in suppression of the observed phased transition and no significant features are observed in the near-equimolar compositions. This lack of any obvious crystallization transitions for the near-equimolar compositions, and the general suppression of any observed $T_{\beta}$ could hypothetically be utilized to select specific electrolyte compositions of this binary mixture which would exhibit purely liquid character, and therefore be used for electrochemical application, even at subzero temperatures. Furthermore, from this suppression of any crystallization features in the DSC traces of near-equimolar formulations, where $x_{IL} = 0.6$ and 0.5, relative to the IL-rich or solvent-rich formulations, the existence of a eutectic formulation in this region may be inferred. However, because of the low-temperature limitations of the measurements described in this work, the specific eutectic formulation and the associated eutectic temperature cannot be observed directly.

**3.2. Volumetric Properties.** The density of the pure components and all mixtures was measured at atmospheric pressure from (293.15−363.15) K and the resulting data are presented in Tables 2−4. Excellent agreement was found

**Table 2. Experimental Density, $\rho$, of the $(x)$[Pyrr$_{14}$][TFSI] − $(1 − x)$Butyronitrile Binary Mixtures Measured as a Function of Formulation and Temperature at 101 kPa**

| $x_{IL}$ | T/K = 293.15 | T/K = 298.15 | T/K = 303.15 | T/K = 313.15 | T/K = 323.15 | T/K = 333.15 |
|---|---|---|---|---|---|---|
| | | | $\rho$/g·cm$^{-3}$ | | | |
| 0.0000 | 0.7911 | 0.7864 | 0.7818 | 0.7724 | 0.763 | 0.7535 |
| 0.1003 | 0.9650 | 0.9604 | 0.9557 | 0.9462 | 0.9368 | 0.9273 |
| 0.1994 | 1.0787 | 1.0743 | 1.0696 | 1.0601 | 1.0507 | 1.0411 |
| 0.3001 | 1.1601 | 1.1554 | 1.1508 | 1.1414 | 1.1321 | 1.1229 |
| 0.4006 | 1.2204 | 1.2161 | 1.2114 | 1.2021 | 1.1929 | 1.1837 |
| 0.4999 | 1.2677 | 1.2632 | 1.2586 | 1.2493 | 1.2402 | 1.2310 |
| 0.6000 | 1.3047 | 1.3000 | 1.2955 | 1.2862 | 1.2772 | 1.2683 |
| 0.7000 | 1.3351 | 1.3305 | 1.326 | 1.3168 | 1.3079 | 1.2989 |
| 0.8000 | 1.3606 | 1.356 | 1.3515 | 1.3423 | 1.3333 | 1.3241 |
| 0.9007 | 1.3820 | 1.3775 | 1.373 | 1.3638 | 1.3549 | 1.3457 |
| 1.0000 | 1.3998 | 1.3952 | 1.3907 | 1.3817 | 1.3728 | 1.3638 |

Standard uncertainties $u$ are $u(T) = 0.01$ K, $u(x_{IL}) = 0.0002$, $u(\rho) = 0.001\rho$ and $u(p) = 2$ kPa.

**Table 3. Experimental Density, $\rho$, of the $(x)$[Pyrr$_{14}$][TFSI] − $(1 − x)$Glutaronitrile Binary Mixtures Measured as a Function of Formulation and Temperature at 101 kPa**

| $x_{IL}$ | T/K = 293.15 | T/K = 298.15 | T/K = 303.15 | T/K = 313.15 | T/K = 323.15 | T/K = 333.15 |
|---|---|---|---|---|---|---|
| | | | $\rho$/g·cm$^{-3}$ | | | |
| 0.0000 | 0.9870 | 0.9831 | 0.9791 | 0.9712 | 0.9634 | 0.9556 |
| 0.1003 | 1.0942 | 1.0903 | 1.0862 | 1.0779 | 1.0697 | 1.0615 |
| 0.1997 | 1.1675 | 1.1633 | 1.1590 | 1.1505 | 1.142 | 1.1337 |
| 0.2999 | 1.2225 | 1.2181 | 1.2138 | 1.2051 | 1.1965 | 1.1880 |
| 0.4002 | 1.2667 | 1.2622 | 1.2579 | 1.2490 | 1.2403 | 1.2317 |
| 0.5006 | 1.3005 | 1.2961 | 1.2917 | 1.2828 | 1.2740 | 1.2652 |
| 0.6003 | 1.3275 | 1.3231 | 1.3186 | 1.3097 | 1.3009 | 1.2919 |
| 0.6998 | 1.3491 | 1.3448 | 1.3403 | 1.3313 | 1.3225 | 1.3138 |
| 0.8004 | 1.3685 | 1.3643 | 1.3598 | 1.3508 | 1.3420 | 1.3330 |
| 0.9002 | 1.3854 | 1.3809 | 1.3764 | 1.3672 | 1.3582 | - |
| 1.0000 | 1.3998 | 1.3952 | 1.3907 | 1.3817 | 1.3728 | 1.3638 |

Standard uncertainties $u$ are $u(T) = 0.01$ K, $u(x_{IL}) = 0.0002$, $u(\rho) = 0.001\rho$ and $u(p) = 2$ kPa.

**Table 4. Experimental Density, $\rho$, of the $(x)$[Pyrr$_{14}$][TFSI] − $(1 − x)$Adiponitrile Binary Mixtures Measured as a Function of Formulation and Temperature at 101 kPa**

| $x_{IL}$ | T/K = 293.15 | T/K = 298.15 | T/K = 303.15 | T/K = 313.15 | T/K = 323.15 | T/K = 333.15 |
|---|---|---|---|---|---|---|
| | | | $\rho$/g·cm$^{-3}$ | | | |
| 0.0000 | 0.9623 | 0.9586 | 0.9548 | 0.9472 | 0.9398 | 0.9323 |
| 0.1002 | 1.0635 | 1.0595 | 1.0556 | 1.0476 | 1.0398 | 1.0319 |
| 0.1996 | 1.1380 | 1.1339 | 1.1298 | 1.1215 | 1.1134 | 1.1054 |
| 0.3004 | 1.1968 | 1.1925 | 1.1883 | 1.1799 | 1.1716 | 1.1633 |
| 0.3995 | 1.2430 | 1.2387 | 1.2344 | 1.2258 | 1.2173 | 1.2063 |
| 0.5001 | 1.2816 | 1.2773 | 1.2729 | 1.2642 | 1.2556 | 1.2468 |
| 0.6000 | 1.3131 | 1.3086 | 1.3042 | 1.2953 | 1.2867 | 1.2779 |
| 0.7011 | 1.3400 | 1.3356 | 1.3312 | 1.3223 | 1.3136 | 1.3047 |
| 0.7996 | 1.3625 | 1.3582 | 1.3538 | 1.3448 | 1.3360 | 1.3267 |
| 0.8997 | 1.3823 | 1.3780 | 1.3735 | 1.3645 | 1.3556 | 1.3463 |
| 1.0000 | 1.3998 | 1.3952 | 1.3907 | 1.3817 | 1.3728 | 1.3638 |

Standard uncertainties $u$ are $u(T) = 0.01$ K, $u(x_{IL}) = 0.0002$, $u(\rho) = 0.001\rho$ and $u(p) = 2$ kPa.

between density data of each pure component measured herein with those available in the literature: that is, <0.1% average deviation between experimental and literature values for [Pyrr$_{14}$][TFSI][37−45] and ADN[11,46−52] and ca. 0.2% deviation for GLN[46−48,53] and BTN.[53−60] The percentage deviations between experimental density values reported in this work for the neat components and those reported previously in the literature are shown in Figures S7 to S10. Furthermore, and as expected, all of the mixtures and single components exhibited a typical linear decrease as a function of increasing temperature. This relationship is used to correlate the temperature dependence of the density of the binary mixtures using eq 1:

$$\rho = \alpha + \beta T \tag{1}$$

where $\rho$ is the density, $T$ is the temperature, and $\alpha$ and $\beta$ are the linear fitting coefficients tabulated in Table S1 in the Supporting Information. This information is presented graphically in Figure S6.

Across the full range of temperatures, addition of the nitrile solvent to the IL results in a nonlinear decrease in measured density. To probe the volumetric effect of combining the two components, the measured densities were used to calculate the excess molar volume, $V_m^E$, across the full range of isotherms, presented as a function of composition in Figure 1. This is achieved by subtracting the ideal molar volume, $V_m^i$, from the experimental molar volume, $V_m^r$, as reported in eq 2:

$$V_m^E = V_m^r - V_m^i = \frac{x_1 M_1 + x_2 M_2}{\rho_{exp}} - \left(\frac{x_1 M_1}{\rho_1} + \frac{x_2 M_2}{\rho_2}\right) \tag{2}$$

where $x_i$ and $M_i$ are the mole fraction and molar mass of components 1 and 2 of the binary mixture, respectively, $\rho_i$ is the density of the pure components 1 and 2, and $\rho_{exp}$ is the experimentally determined density of the binary mixture.

Additionally, the calculated numerical values of $V_m^E$ are presented in Tables S2 to S4. The uncertainty in the calculated excess molar volume data was estimated, by the propagation of errors, to be approximately $\pm 9 \times 10^{-2}$ cm$^3$·mol$^{-1}$.
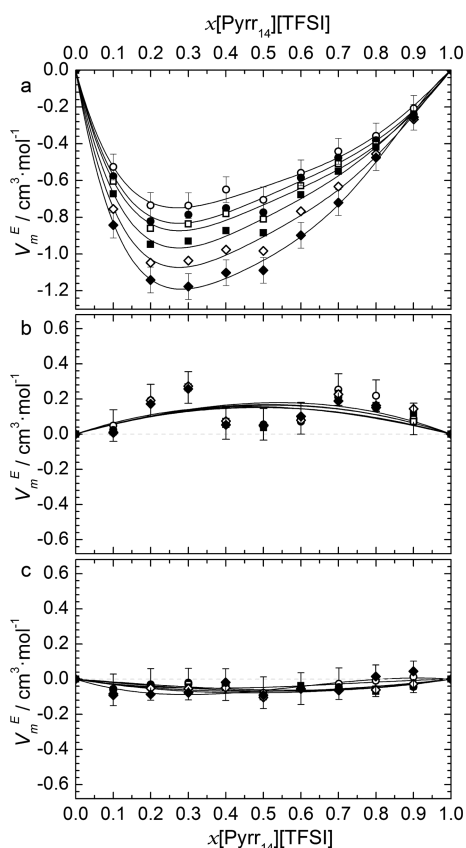
**Figure 1.** Excess molar volumes of the $(x)[\text{Pyrr}_{14}][\text{TFSI}] - (1 - x)$ nitrile binary mixture containing butyronitrile (a), glutaronitrile (b), and adiponitrile (c) at 293.15 K, ○; 298.15 K, ●; 303.15 K, □; 313.15 K, ■; 323.15 K, ◇; and 333.15 K, ◆. The solid lines represent the calculated correlation by the Redlich−Kister expansion using eq 3 with parameters reported in Table 5 for BTN mixtures and Table S5 for GLN and ADN mixtures.

With regards to the BTN-containing mixtures (Figure 1a), the calculated excess molar volume is found to be negative across the full range of binary compositions and across the full temperature range, indicating a contraction of the volume occupied relative to the ideal volume determined from the molar volume of the two pure components. This may occur through strong interactions being more favorable between unlike molecules (i.e., BTN-IL interactions and not BTN-BTN or IL-IL interactions) and/or more efficient packing of the components.

The calculated excess molar volume is found to increase slightly with the increase in temperature from (293.15 to 333.15) K and to be asymmetrical as the minimum is observed, whatever the temperature, in the solvent-rich region (ca. $x[\text{Pyrr}_{14}][\text{TFSI}] \approx 0.3$). Furthermore, for each isotherm of the BTN-containing mixtures, the excess molar volume data were then satisfactorily correlated by a third order Redlich−Kister polynomial expansion (eq 3; where $j = 3$) as shown in Figure 1a.

$$\lambda_{\text{calc}} = x_1 x_2 \sum_{k=0}^{j} A_k (x_1 - x_2)^k \tag{3}$$

where $A_k$ represents the coefficient of the polynomial of the order $k$ and $j$ represents the upper limit of the expansion. The fitting coefficients are presented in Table 5 with the standard

**Table 5. Coefficients of the Redlich−Kister Polynomial Expansion, $A_k$, and the Respective Standard Deviations, $\sigma_{\text{SD}}$, for the Excess Molar Volume, $V_m^E$, of the Binary Mixture $(x)[\text{Pyrr}_{14}][\text{TFSI}] - (1 - x)$Butyronitrile**

| $T/\text{K}$ | $A_0$ | $A_1$ | $A_2$ | $A_3$ | $\sigma_{\text{SD}}$ |
|---|---|---|---|---|---|
| 293.15 | −2.540 | 1.381 | −2.283 | 1.437 | 0.04 |
| 298.15 | −2.775 | 1.766 | −2.537 | 1.056 | 0.04 |
| 303.15 | −2.932 | 1.773 | −2.662 | 1.248 | 0.04 |
| 313.15 | −3.230 | 2.060 | −2.696 | 1.614 | 0.04 |
| 323.15 | −3.624 | 2.168 | −2.936 | 2.074 | 0.04 |
| 333.15 | −4.137 | 2.242 | −2.728 | 3.031 | 0.03 |

deviation, $\sigma_{\text{SD}}$, of this correlation. The standard deviation is calculated using the eq 4.

$$\sigma_{\text{SD}} = \left[ \frac{\sum (\lambda_{\text{exp}} - \lambda_{\text{calc}})^2}{n - p} \right]^{0.5} \tag{4}$$

where $\lambda_{\text{exp}}$ represents the experimentally determined value (excess molar volume, $V_{m,\text{exp}}^E$, in this instance), $\lambda_{\text{calc}}$ represents the respective value as calculated by eq 4 ($V_{m,\text{calc}}^E$ in this instance), $n$ is the number of experimental data points, and $p$ is the number of coefficients used in the correlation.

For the two binary mixtures containing the dinitrile solvents, GLN and ADN, the trends in the excess volumetric properties are not as prominent as seen in the BTN system. Plots of the excess molar volume of the GLN and ADN binary systems are shown in Figure 1 panels b and c, respectively. Very small deviations from ideal mixing (where $V_m^E \approx 0 \text{ cm}^3 \cdot \text{mol}^{-1}$) are observed and, as such, the associated errors in the calculations become very significant and it is difficult to accurately probe the behaviors of these systems. To more accurately determine these minute changes, initial measurements of the density should be completed using a densitometer with a higher degree of accuracy. However, since the calculated values are very small it may be qualitatively inferred that the dinitrile solvents interact in a different manner with the IL when compared to the BTN solvent. Nevertheless, the excess molar volume data for the two dinitrile-containing mixtures was correlated using a first order Redlich−Kister expansion (eq 3; where $j = 1$). The respective fitting coefficients, $A_k$, and the calculated standard deviations, $\sigma_{\text{SD}}$, are presented in Table S5.

The lack of any significant deviation away for $V_m^E$ is markedly different from previous reports of the excess molar volume of binary mixtures containing ADN and [EMIm][TFSI], in which relatively large negative deviations were observed.[11] However, although the same anion was present here, the aromatic imidazolium cation would be expected to interact with the solvent differently and strongly through $\pi - \pi$ interactions in the solution.

**3.3. Viscosity.** The viscosity of the pure components and all mixtures was measured at atmospheric pressure from (293.15−333.15) K and the resulting data is presented in Tables 6−8. The viscosity of electrolytes is an important feature, linked to the diffusivity of the components, for energy storage devices. This is particularly true for EDLCs where high currents and high power capabilities relate to the ability of ions to move quickly to and from the electrode interface. The viscosity of the pure IL (77.7 mPa·s at 298.15 K) has been measured many times previously, and the values reported here are in good agreement with values in the literature (ca. 0.2−2% deviation between experimental and literature values).[35,37,38,40,42−45] The

**Table 6. Experimental Viscosity, $\eta$, of the $(x)[\mathrm{Pyrr}_{14}][\mathrm{TFSI}]$ $- (1 - x)$Butyronitrile Binary Mixtures Measured as a Function of Formulation and Temperature at 101 kPa**

| $x_{\mathrm{IL}}$ | T/K = 293.15 | T/K = 298.15 | T/K = 303.15 | T/K = 313.15 | T/K = 323.15 | T/K = 333.15 |
|---|---|---|---|---|---|---|
| | | | $\eta$/mPa·s | | | |
| 0.0000 | *0.88* | *0.86* | *0.84* | *0.81* | *0.78* | *0.75* |
| 0.1009 | *1.51* | *1.45* | *1.37* | *1.25* | *1.17* | *1.12* |
| 0.1987 | 2.73 | 2.53 | 2.37 | 2.07 | *1.84* | *1.65* |
| 0.3002 | 6.43 | 5.72 | 5.13 | 4.22 | 3.52 | 3.03 |
| 0.4000 | 8.77 | 7.81 | 7.14 | 5.68 | 4.62 | 3.85 |
| 0.5012 | 14.45 | 12.44 | 10.81 | 8.38 | 6.67 | 5.43 |
| 0.6000 | 22.39 | 18.94 | 16.20 | 12.18 | 9.47 | 7.55 |
| 0.7000 | 33.65 | 27.95 | 23.51 | 17.18 | 13.04 | 10.20 |
| 0.8000 | 49.94 | 40.71 | 33.68 | 23.91 | 17.69 | 13.55 |
| 0.9000 | 73.01 | 58.33 | 47.41 | 32.67 | 23.59 | 17.71 |
| 1.0000 | 98.72 | 77.66 | 62.29 | 41.87 | 29.61 | 21.82 |

Standard uncertainties $u$ are $u(T)$ = 0.05 K, $u(x_{\mathrm{IL}})$ = 0.0002, $u(\eta)$ = $0.03\eta$ and $u(p)$ = 2 kPa. Values which fall below the measurable range of the device (i.e., < 2.5 mPa·s) are shown in bold italics to highlight significant inaccuracy of these measurements (e.g., the viscosity of pure BTN is 0.55 mPa·s at 298 K).[54]

**Table 7. Experimental Viscosity, $\eta$, of the $(x)[\mathrm{Pyrr}_{14}][\mathrm{TFSI}]$ $- (1 - x)$Glutaronitrile Binary Mixtures Measured as a Function of Formulation and Temperature at 101 kPa**

| $x_{\mathrm{IL}}$ | T/K = 293.15 | T/K = 298.15 | T/K = 303.15 | T/K = 313.15 | T/K = 323.15 | T/K = 333.15 |
|---|---|---|---|---|---|---|
| | | | $\eta$/mPa·s | | | |
| 0.0000 | 6.97 | 6.12 | 5.39 | 4.25 | 3.47 | 2.88 |
| 0.1003 | 9.92 | 8.55 | 7.42 | 5.78 | 4.60 | 3.72 |
| 0.1997 | 13.34 | 11.42 | 9.83 | 7.46 | 5.84 | 4.71 |
| 0.2999 | 17.57 | 14.81 | 12.69 | 9.52 | 7.39 | 5.85 |
| 0.4002 | 22.88 | 19.17 | 16.22 | 11.97 | 9.16 | 7.27 |
| 0.5006 | 28.92 | 23.95 | 20.10 | 14.66 | 11.11 | 8.67 |
| 0.6003 | 38.47 | 31.50 | 26.13 | 18.67 | 13.88 | 10.69 |
| 0.6998 | 48.33 | 39.56 | 32.56 | 22.97 | 16.93 | 13.01 |
| 0.8004 | 61.37 | 49.40 | 40.38 | 28.01 | 18.72 | 14.20 |
| 0.9002 | 78.19 | 62.15 | 50.27 | 34.37 | 24.65 | 18.39 |
| 1.0000 | 98.72 | 77.66 | 62.29 | 41.87 | 29.61 | 21.82 |

Standard uncertainties $u$ are $u(T)$ = 0.05 K, $u(x_{\mathrm{IL}})$ = 0.0002, $u(\eta)$ = $0.03\eta$ and $u(p)$ = 2 kPa.

**Table 8. Experimental Viscosity, $\eta$, of the $(x)[\mathrm{Pyrr}_{14}][\mathrm{TFSI}]$ $- (1 - x)$Adiponitrile Binary Mixtures Measured as a Function of Formulation and Temperature at 101 kPa**

| $x_{\mathrm{IL}}$ | T/K = 293.15 | T/K = 298.15 | T/K = 303.15 | T/K = 313.15 | T/K = 323.15 | T/K = 333.15 |
|---|---|---|---|---|---|---|
| | | | $\eta$/mPa·s | | | |
| 0.0000 | 7.17 | 6.31 | 5.53 | 4.54 | 3.73 | 3.02 |
| 0.1002 | 9.85 | 8.45 | 7.35 | 5.72 | 4.53 | 3.74 |
| 0.1996 | 13.22 | 11.27 | 9.71 | 7.43 | 5.86 | 4.80 |
| 0.3004 | 17.56 | 14.79 | 12.61 | 9.44 | 7.32 | 5.87 |
| 0.3995 | 25.01 | 21.46 | 18.54 | 14.05 | 10.01 | 7.86 |
| 0.5001 | 31.00 | 25.62 | 21.53 | 15.63 | 11.82 | 9.21 |
| 0.6000 | 37.48 | 30.92 | 25.59 | 18.34 | 13.70 | 10.59 |
| 0.7011 | 48.32 | 39.22 | 32.33 | 22.83 | 16.83 | 12.85 |
| 0.7996 | 59.96 | 48.21 | 39.41 | 27.42 | 19.97 | 15.09 |
| 0.8997 | 77.23 | 61.49 | 49.74 | 34.01 | 24.42 | 18.22 |
| 1.0000 | 98.72 | 77.66 | 62.29 | 41.87 | 29.61 | 21.82 |

Standard uncertainties $u$ are $u(T)$ = 0.05 K, $u(x_{\mathrm{IL}})$ = 0.0002, $u(\eta)$ = $0.03\eta$ and $u(p)$ = 2 kPa.

and those reported previously in the literature are summarized in Figures S11 to S14.

As is expected for the binary mixtures, addition of the lower viscosity molecular solvents to the IL results in a nonlinear reduction in the viscosity with respect to the molar fraction of the two components. Additionally, for these binary mixtures, an increase in the temperature resulted in a nonlinear decrease in the measured viscosity across the full range of compositions. The most significant reductions in viscosity relative to the neat IL are observed at lower temperatures, such that the viscosity of the mixtures and neat components begin to converge at higher temperatures. In turn, the relative variation in viscosity as a function of temperature is greatest for the neat IL (and lowest for the neat molecular solvents) in all cases. In fact, for the mononitrile solvent, BTN, the variation in measured viscosity is very small (0.88 mPa·s at 293.15 K to 0.75 mPa·s at 333.15 K) and, as such, the temperature dependence appears almost linear over the studied temperature range, though the aforementioned limitation of the accuracy within this viscosity range makes asserting particular trends difficult for this sample. However, in the context of electrolytes, the measurements show that high nitrile molecular solvent fractions are important for attaining low viscosity (and high mobility) liquids capable of supporting rapid electrochemical processes. Nevertheless, as discussed, the viscosity is just one of many important properties in the overall performance and safety of the electrolytes.

The temperature dependencies of the viscosity of all studied compositions are presented in Figure 2. Additionally, the temperature dependence of the viscosity, $\eta$, is correlated using the Arrhenius equation:

$$\eta = A_\eta \, \exp\!\left(\frac{E_a^\eta}{RT}\right) \tag{5}$$

where $A_\eta$ is the pre-exponential factor, $E_a^\eta$ is the activation energy of viscous flow, and $R$ is the gas constant (8.3145 J·mol$^{-1}$·K$^{-1}$), and by the Vogel−Tammann−Fulcher (VTF) equation:

$$\eta = \eta_{\mathrm{o}} \, \exp\!\left(\frac{B_\eta}{T - T_{\mathrm{o}}^\eta}\right) \tag{6}$$

viscosity data of the pure dinitrile solvents, although less readily found in the literature, are considered in reasonable agreement with the available data, GLN[29,47,61] and ADN.[11,47,49,50,52] However, the measured viscosity of the pure BTN (0.8 mPa·s at 298.15 K) appears to be overestimated across the full temperature range when compared to reference values (0.55 mPa·s at 298.15 K).[54,56,60] While the absolute difference is small (ca. 0.25 mPa·s), the relative difference is over 30% at 298 K and most significant for the neat mononitrile solvent. This error is due to the accuracy limitation of the particular capillary used in the falling/rolling ball viscometer. These capillaries are calibrated for a range of viscosities (2.5−70 mPa·s) and the viscosity, or lack thereof, of the pure BTN falls outside of this range. Additionally, any such values which fall below this viscosity range are shown clearly in bold italics in Table 6 to highlight values where the uncertainty in the measurement is large. The percentage deviations between experimental viscosity values reported in this work for the neat components

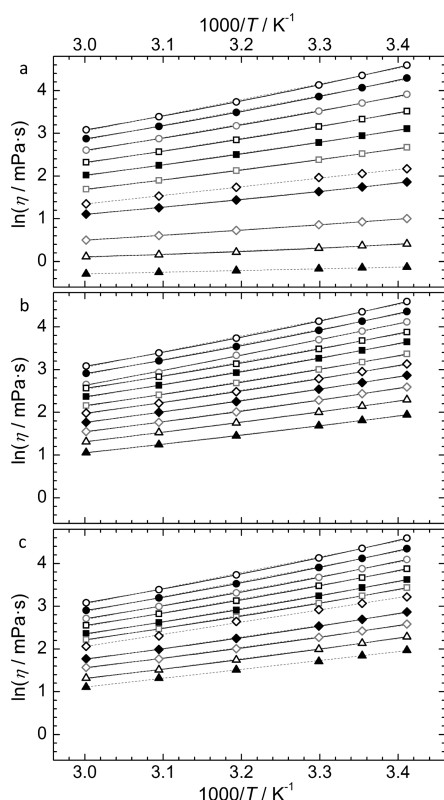**Figure 2.** Temperature dependence of the viscosity of the range of $[Pyrr_{14}][TFSI]$ binary mixtures with butyronitrile (a), glutaronitrile (b), and adiponitrile (c) where the symbol represents the molar fraction of the IL, $x[Pyrr_{14}][TFSI]$: $x = 0$, ▲; 0.1, △; 0.2, gray ◇; 0.3, ◆; 0.4, ◇; 0.5, gray □; 0.6, ■; 0.7, □; 0.8, gray ○; 0.9, ●; 1, ○. Solid black lines and dashed gray lines represent the correlation of the data by the VTF equation and the Arrhenius equation, respectively. Accurate molar fractions of the components of the three binary mixtures match those provided in Tables 6−8

where $\eta_o$ is the limiting viscosity and $B_\eta$ and $T_o^\eta$ are fitting parameters related to the pseudoactivation energy and glass transition temperature, respectively. The VTF equation is commonly used to describe the temperature−viscosity relationship in glassy-forming liquids such as ILs which typically do not follow Arrhenius dependence. The fitting parameters for both methods are shown in Tables S6 to S8. Relative to the viscosity of the pure IL, addition of the BTN yields the greatest reduction in the viscosity compared to the other nitrile solvents reported here. This is expected since the viscosity of the pure mononitrile solvent is an order of magnitude lower than for the dinitriles. Furthermore, the reduction in viscosity upon addition of solvent is practically identical when comparing the two dinitrile species owing to likely very similar neat viscosities and very similar solvent/IL interactions.

The measured viscosity of the binary mixtures was used to calculate viscosity deviations from ideality, $\Delta\eta$, using the equation:

$$\Delta\eta = \eta - (x_1\eta_1 + x_2\eta_2) \tag{7}$$

where $x_i$ is the mole fraction of components 1 and 2 and $\eta_i$ and $\eta$ are the viscosities of the pure components 1 and 2 and of the binary mixtures, respectively. The calculated $\Delta\eta$ values for the three $(x)[Pyrr_{14}][TFSI] - (1 - x)nitrile$ mixtures are presented in Figure 3a−c as functions of composition and temperature. It can be seen that all calculated $\Delta\eta$ values are negative across the

full temperature and composition range and exhibit asymmetric minima at approximately $x[Pyrr_{14}][TFSI] = 0.6$. Furthermore, for all three binary mixtures, $\Delta\eta$ values decrease upon increasing temperature. Considering the magnitudes of the observed viscosity deviations for the three different binary mixtures, it is immediately clear that the largest deviations are observed for the BTN-containing mixtures (where the minimum $\Delta\eta$ = ca. −35 mPa·s at 293 K and $x[Pyrr_{14}][TFSI]$ = 0.6). The two dinitrile solvents exhibit very similar, smaller magnitudes of $\Delta\eta$ (where the minima $\Delta\eta$ = ca. −24 mPa·s and −25 mPa·s at 293 K and $x[Pyrr_{14}][TFSI]$ = 0.6 for the GLN and ADN-containing mixtures, respectively).

Utilizing the viscosities and molar volumes of the pure components and the respective mixtures, the excess Gibbs energy of activation of viscous flow is calculated for the three binary mixtures using the equation:

$$\frac{\Delta G^{E*}}{RT} = \left[\ln\left(\frac{\eta V_m}{\eta_2 V_{m,2}}\right) - x_1\ln\left(\frac{\eta_1 V_{m,1}}{\eta_2 V_{m,2}}\right)\right] \tag{8}$$

where $R$ is the gas constant, $T$ is the sample temperature, $\eta$ and $V_m$ are the viscosity and molar volume of the mixture, respectively, at a given mole fraction of component 1, $x_1$, and $\eta_i$ and $V_{m,i}$ are the viscosities and molar volumes, respectively, of the pure components. The calculated $\Delta G^{E*}$ values for the three $(x)[Pyrr_{14}][TFSI] - (1 - x)nitrile$ mixtures are presented in Figure 3d−f as functions of composition and temperature. Both the viscosity deviations from ideality and the excess Gibbs energies of activation of viscous flow were correlated by first order Redlich−Kister type expansions (eq 3; where $j = 1$) and the standard deviation of the correlation, $\sigma_{SD}$, was calculated by eq 4, where $\lambda_{exp}$ represent $\Delta\eta$ or $\Delta G^{E*}$ values as calculated by eqs 7 and 8, respectively, and $\lambda_{calc}$ represents $\Delta\eta$ or $\Delta G^{E*}$ values as calculated by eq 3. All numerical values for $\Delta\eta$ and $\Delta G^{E*}$, and the respective coefficients of Redlich−Kister correlations and standard deviations, are presented in Tables S9 to S14. By propagation of errors from eq 8, the uncertainty in $\Delta G^{E*}$ can be approximated as ca. ±5%, and while several points shown in Figure 3 panels d and f lie above the solid line of the simple first-order Redlich−Kister correlation, the overall trends in activation energies for the three mixtures are clear.

For all three binary mixtures, all $\Delta G^{E*}$ values are positive across the full temperature and composition range. The nature of the positive values for $\Delta G^{E*}$ across the full composition ranges are indicative of adhesive interactions or complex formation between unlike constituents of the mixture.[62,63] The magnitude of calculated $\Delta G^{E*}$ values is greatest for the BTN-containing binary mixtures, supporting the excess volumetric properties presented in Figure 1a, indicative of significant adhesive interactions between IL and mononitrile solvent. Strong positive deviations in $\Delta G^{E*}$ have been reported previously for IL binary mixtures with ACN,[64] and short-chain alcohols,[65] generally attributed to intermolecular hydrogen bonding. As observed with the excess molar volumes of the dinitrile solvent-containing binary mixtures, the magnitude of deviations from ideality is significantly lower. Furthermore, taking into consideration the aforementioned accuracy limitations of the viscosity of the neat BTN, the calculated $\Delta G^{E*}$ values for the BTN-containing mixtures appear underestimated. Calculation of $\Delta G^{E*}$ values using a literature value for the viscosity of BTN (0.55 mPa·s at 298 K)[54] results in a slight shift in the apparent maximum toward more solvent-rich formulations and increase in the magnitude of the maximum,
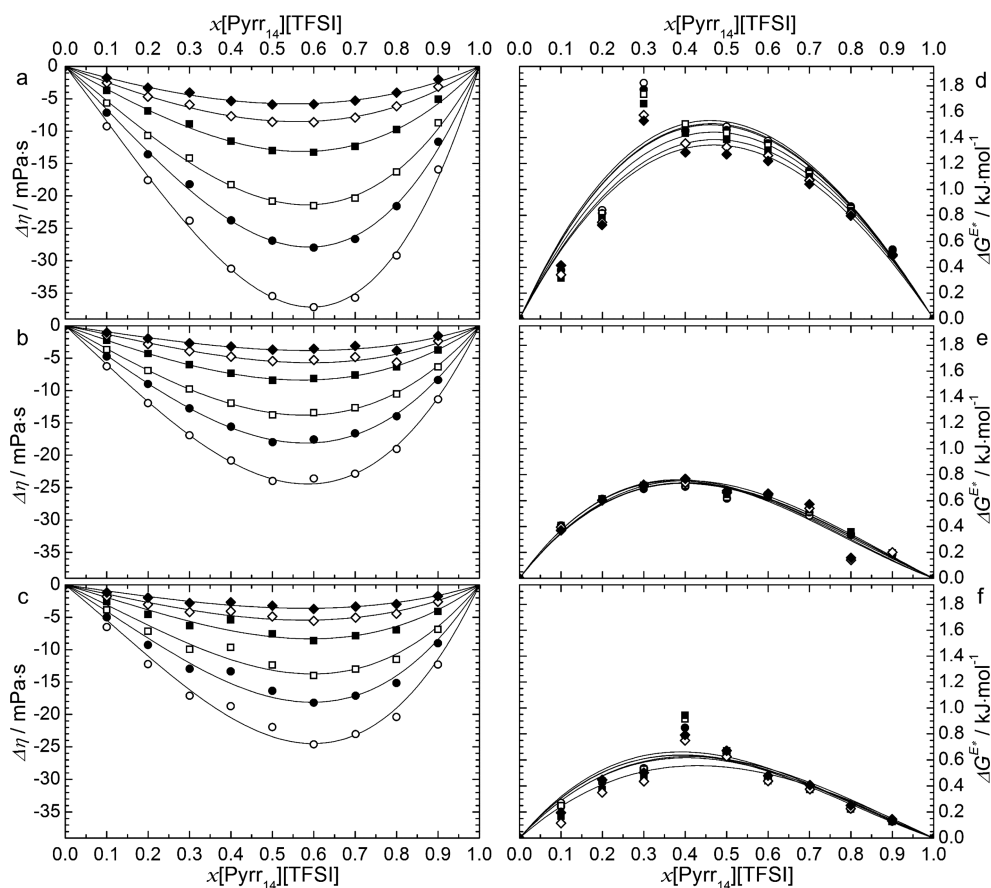
**Figure 3.** Viscosity deviations from ideality, $\Delta\eta$, (a−c) and excess Gibbs activation energy of viscous flow, $\Delta G^{E*}$, (d−f) for the $(x)[\text{Pyrr}_{14}][\text{TFSI}] - (1-x)nitrile$ binary mixture containing butyronitrile (a, d), glutaronitrile (b, e), and adiponitrile (c, f) at 293.15 K, $\bigcirc$; 298.15 K, $\bullet$; 303.15 K, $\square$; 313.15 K, $\blacksquare$; 323.15 K, $\diamondsuit$; and 333.15 K, $\blacklozenge$. The solid lines represent correlation of the data by first order Redlich−Kister expansion. Accurate molar fractions of the components of the three binary mixtures match those provided in Tables 6−8.
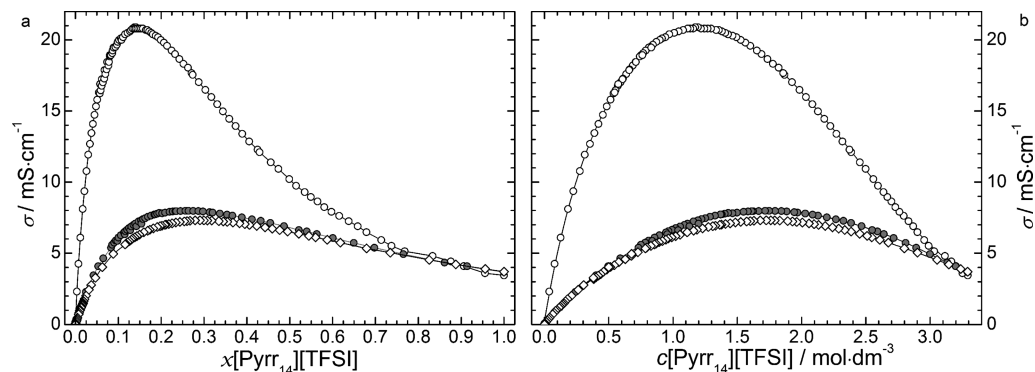


**Figure 4.** Conductivity, $\sigma$, of the three binary mixtures containing butyronitrile ($\bigcirc$), glutaronitrile ($\bullet$), and adiponitrile ($\diamondsuit$) as a function of (a) the molar fraction of IL, $x[\text{Pyrr}_{14}][\text{TFSI}]$, and (b) the concentration of IL, $c[\text{Pyrr}_{14}][\text{TFSI}]$, at 305 ± 1 K.

from ca. 1.4 kJ·mol$^{-1}$ to 2.2 kJ·mol$^{-1}$, further supporting the evidence of the strong interactions in these mixtures. Conversely, the $\Delta\eta$ values for these mixtures show very little deviation (generally <1%) when calculated using the literature data or the values reported in this work.

All of the evidence presented in sections 3.2 and 3.3 indicate the presence of significant associative interactions between the smaller, mononitrile solvent, BTN, and the IL. Conversely, the data presented for the mixtures containing dinitrile solvents, GLN and ADN, indicate quasi-ideal type behavior for the measured properties on mixing. In terms of intermolecular associations in BTN-containing mixtures, this may be related to the reasonably strong, unilateral dipole moment of the single CN bond (3.9 D)[66] freely associating with the IL; possibly through the partially positive $\alpha$-protons next to the nitrogen center of the pyrrolidinium cation and the partially negative nitrogen of the CN bond in BTN. For the dinitrile solvents, the dipole moment of each CN bond is essentially opposed by an equivalent dipole in an opposite direction. This affects a lack of interaction between solvent and IL constituents and, therefore, inhibits restructuring of the components upon mixing which is observed through a quasi-ideal response.

**3.4. Conductivity.** As described in the experimental section, the conductivity of the binary mixtures was first measured as a function of the formulation by continuous addition of small amounts of the one component to a fixed quantity of the second component. The masses of both components are accurately recorded and the conductivity is measured once a homogeneous mixture is achieved. The measurements were conducted inside a dry Ar-filled glovebox to prevent contamination by water from the atmosphere. As such, the temperature of the measurements, 305 ± 1 K, was dictated by the internal glovebox atmosphere.

The conductivities, $\sigma$, of the three binary mixtures are presented as a function of molar fraction, $x[Pyrr_{14}][TFSI]$, and the concentration, $c[Pyrr_{14}][TFSI]$, of the IL in Figure 4. The concentration of the individual points was estimated from the molar fraction data using a polynomial fit for the variation of density as a function of molar fraction of each of the three respective solvents. The concentration of pure $[Pyrr_{14}][TFSI]$ is approximately 3.29 mol·dm$^{-3}$ at this temperature. As expected, the results show that addition of the nitrile solvents to the neat IL result in a promotion of the exhibited conductivity. This is in accordance with the observed reduction in viscosity, and an associated increase in the mobility of the ionic charge carrying species, relative to the neat IL. All three mixtures show asymmetric maxima in the solvent-rich region where $x[Pyrr_{14}][TFSI]$ = 0.14, 0.26, and 0.29 for the BTN, GLN, and ADN containing binary mixtures, respectively. At more solvent-rich compositions beyond the observed maxima, the concentration of charge carrying ionic species drops to become very dilute and the measured conductivity decreases toward the insulating nature of the pure solvent species.

The trends in the magnitude of the observed maxima is in good agreement with the relative viscosities of the binary mixtures reported in section 3.3; that is, the BTN mixtures exhibit the lowest viscosity and highest conductivity (20.9 mS·cm$^{-1}$) formulation while the dinitrile-containing mixtures exhibit higher viscosity and much lower conductivity (7.98 mS·cm$^{-1}$ and 7.31 mS·cm$^{-1}$ for the GLN and ADN mixtures, respectively). Additionally, the position and magnitude of the maxima observed for the BTN mixture is in reasonable agreement with a previous report.[9] While the data presented in Figure 4b provides the same results and trends as Figure 4a, it highlights the particular benefits of being able to use higher salt concentrations when using IL salts in EDLC electrolytes (and allows comparison with some conventional EDLC electrolytes). Higher salt concentrations can, in some cases, be utilized to achieve higher conductivities than may be possible with a non-IL salt before saturation is reached and may limit the effect of ion depletion at the electrode/electrolyte interface during cycling of the EDLC device.[3] Additionally, due to the typically negligible vapor pressure of ILs, further addition of IL to the binary mixture will effectively reduce the apparent vapor pressure of the mixture, according to the Raoult's law, while still maintaining an entirely liquid phase. Considering the volatile nature of PC and ACN, lowering the volatility is a key factor for the development of safer EDLC electrolytes in the future. In fact, the significant cohesive or associative interactions in the BTN-containing mixtures inferred from the previous sections would indicate a strong probability of significant negative deviations from Raoult's Law, and effective suppression of the electrolyte vapor pressure (relative to pure BTN), for these mixtures. For example, strong negative deviations from Raoult's Law, and significant reductions in solvent vapor pressure, for

binary mixtures containing ACN and $[BMIm][BF_4]$ have been reported,[67] and the deviations in the excess molar volume of equivalent mixtures are also reported, separately, to be negative across the full composition range.[68] Conversely, the quasi-ideal mixing interactions indicated for the dinitrile-containing mixtures would suggest the probability of any deviations in Raoult's Law for these mixtures would be less significant.

In comparison to the conductivity of conventional EDLC electrolytes, for example, 1 mol·dm$^{-3}$ $[Et_4N][BF_4]$ in ACN (56 mS·cm$^{-1}$ at 298 K) or PC (13 mS·cm$^{-1}$ at 298 K),[69] the low viscosity mixtures with BTN exhibit good conductivities (e.g., > 10 mS·cm$^{-1}$) comparable to PC-based analogues between the range of ca. 0.3 to 2.5 mol·dm$^{-3}$. While the ACN equivalents exhibit considerably higher conductivities than is observed for any mixtures studied here, it should be noted that the trade-off between high-transport properties (in the case of ACN) and lower volatility (in the case of BTN, and even more so in the case of the dinitriles) is very important in the balance between applicability of the systems and their safety.

For further characterization, the composition of the binary mixtures which exhibited the maximum conductivity, $\sigma_{max}$, is utilized. First, the conductivity of the three $\sigma_{max}$ compositions and the neat IL was measured as a function of temperature within the range of (293−333) K and the results are presented in Figure 5. The numerical data is given in Table S15. The
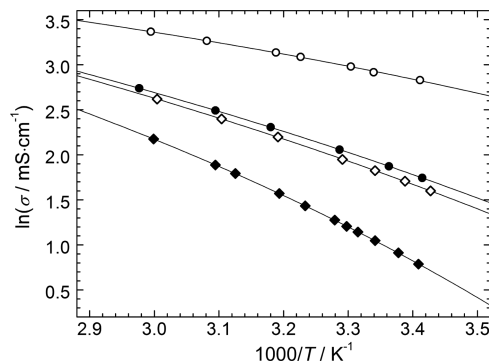


**Figure 5.** Temperature dependence of conductivity of the $\sigma_{max}$ compositions of the $[Pyrr_{14}][TFSI]$ binary mixtures with butyronitrile (○), glutaronitrile (●), and adiponitrile (◇) and for the neat $[Pyrr_{14}][TFSI]$ (◆). Solid lines represent the correlation of the data by the VTF equation.

conductivity of the neat IL within this temperature range is also presented for comparison. The conductivity of the neat IL is across the measured temperature range is in good agreement with values previously reported in the literature (ca. < 2% average deviation) and a graphical representation of the percentage deviations is shown in Figure S15 in the ESI.[37,42−44] Additionally, similar to the viscosity of the IL and IL/nitrile mixtures, the temperature dependence of the conductivity was correlated using an analogous version of the VTF equation:

$$\sigma = \sigma_o \exp\left(\frac{-B_\sigma}{T - T_o^\sigma}\right) \tag{9}$$

where $\sigma_o$ is the limiting conductivity and $B_\sigma$ and $T_o^\sigma$ are fitting parameters related to the pseudoactivation energy for conduction and the glass-transition temperature, respectively. Good correlation is achieved, as shown by the solid lines in Figure 5, for the neat IL and the binary mixtures and the

numerical fitting parameters, $\sigma_o$, $B_\sigma$ and $T_o^\sigma$, are shown in Table S16. The gradients of the temperature dependencies presented in Figure 5 show that a greater relative promotion of the ionic conductivity is observed for the neat IL compared to the IL/nitrile binary mixtures. This is associated with the greater relative promotion in the mobility of the ionic species as the temperature increases and the viscosity of the IL rapidly decreases.

**3.5. Ionicity.** To further inspect the properties of the binary mixtures described in this work, the apparent relationship between the measured viscosities and conductivities of the electrolyte solutions is investigated. The Walden plot for the three binary mixtures at the $\sigma_{max}$ formulations and the neat IL within a temperature range of (293 to 333) K is presented in Figure 6. The concentration (used to calculate the molar
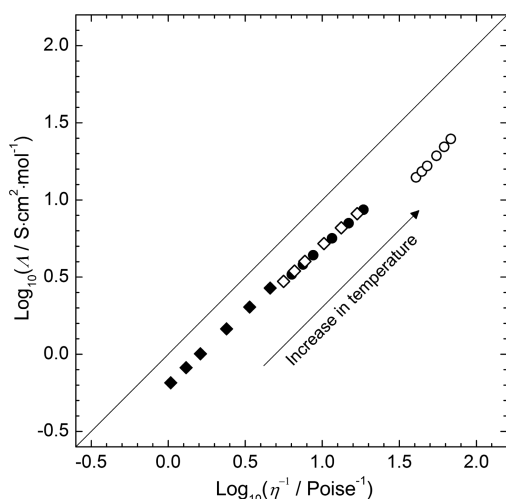


**Figure 6.** Walden plot of the $\sigma_{max}$ compositions of the $[Pyrr_{14}][TFSI]$ binary mixtures with butyronitrile ($\bigcirc$), glutaronitrile ($\bullet$), and adiponitrile ($\diamondsuit$) and for the neat $[Pyrr_{14}][TFSI]$ ($\blacklozenge$) within a temperature range of 293 to 333 K. The solid line represents the ideal Walden behavior of a 0.01 mol·dm$^{-3}$ aqueous solution of KCl.

conductivity, $\Lambda$ [S·cm$^2$·mol$^{-1}$]) of IL in the mixtures was calculated using the measured density of the mixtures (Tables 2−4) and the molar mass of the IL. The specific points on the graph were calculated using the correlation parameters of the fitting equations for conductivity and viscosity measurements. The solid line in the Walden plot represents a so-called *ideal KCl line*, that is, the ideal Walden behavior of a 0.01 mol·dm$^{-3}$ aqueous solution of KCl, a strong electrolyte, where the constituent ions are known to be fully dissociated and equally mobile in solution.[70]

For pure ILs, deviation below this is indicative of a degree of association between the components of the IL, that is, not all ionic species are available for the conduction of charge and the apparent electrolytic conductivity of the IL is lower than may be expected for a given viscosity. The Walden behavior for $[Pyrr_{14}][TFSI]$, as represented by the filled diamonds in Figure 6, shows that this IL lies slightly below the ideal KCl line across the full temperature range. This observation implies a slight tendency for the formation of ion pairs. However, the magnitude of the deviation, $\Delta W$, for this IL is small ($\Delta W <$ 0.3) across the studied temperature range and, therefore, the IL may be considered mostly dissociated and ionic in character in which the mobility of the constituent ions is mostly independent. Conversely, larger deviations below the ideal

KCl line, for example where $\Delta W > 1$, have been for reported for some IL species which exhibit considerably lower conductivities for a given viscosity, typically classed as *poor ionic liquids*.[71,72] Through various interionic associations, the ionic and conductive nature of these ILs is suppressed by the tendency of the materials to form ion pairs.

For the $\sigma_{max}$ compositions of the three studied binary mixtures, the Walden data points are shifted toward the right upper corner of the graph, associated with the reduced viscosity and enhanced conductivity of the binary mixtures relative to the neat IL. Nevertheless, the relative deviation from ideal Walden behavior certainly appears solvent-dependent. The calculated Walden product, $\Lambda \cdot \eta$, for the three mixtures and the neat IL is shown in Table 9. The Walden product is equal to 1 Poise·S·

**Table 9. Walden Product, $\Lambda \cdot \eta$, of the Neat IL and the Three $\sigma_{max}$ Compositions of the Binary Mixtures as a Function of Temperature**

| | $\Lambda \cdot \eta / 10^{-6}$ S·N·s·mol$^{-1}$ | | | |
|---|---|---|---|---|
| $T/K$ | Neat $[Pyrr_{14}]$ $[TFSI]$ | $[Pyrr_{14}]$ $[TFSI]/BTN$ | $[Pyrr_{14}]$ $[TFSI]/GLN$ | $[Pyrr_{14}]$ $[TFSI]/ADN$ |
| 293 | 6.28 | 3.45 | 5.19 | 5.29 |
| 298 | 6.26 | 3.45 | 5.09 | 5.24 |
| 303 | 6.22 | 3.46 | 5.01 | 5.19 |
| 313 | 6.11 | 3.51 | 4.88 | 5.08 |
| 323 | 5.98 | 3.57 | 4.77 | 4.96 |
| 333 | 5.85 | 3.64 | 4.68 | 4.84 |

cm$^2$·mol$^{-1}$ (or $10 \times 10^{-6}$ S·N·s·mol$^{-1}$) for any point on the ideal KCl line and, therefore, values less than this represent deviations below ideal Walden behavior. The value calculated for pure $[Pyrr_{14}][TFSI]$ at 298 K ($6.26 \times 10^{-6}$ S·N·s·mol$^{-1}$) is comparable to a previously reported value for the same IL ($5.6 \times 10^{-6}$ S·N·s·mol$^{-1}$).[73]

As can be seen from the data presented in Table 9 and Figure 6, the presence of the dinitrile solvents, ADN and GLN, has very little effect on the apparent ionicity character of the ionic solution, such that the differences between the deviations from ideality in the neat IL and the binary mixtures are minimal. A more significant variation, that is, a larger negative deviation away from the ideal KCl line, is obvious for the butyronitrile containing mixture. This highlights that the promotion in measured conductivity for the BTN blends is much less than may be expected from the considerable reduction in viscosity according to the Walden rule.

The fact that this behavior is more significant for the mononitrile solvent than for the two dinitrile solvents may link to excess volumetric properties of the binary mixtures (see section 3.2). The BTN containing binary mixtures exhibited negative deviations from ideal mixing across all formulations which implies a volume contraction due to associative forces or more efficient packing of the materials upon mixing (Figure 1a). If this feature was attributed primarily to adhesive interactions between unlike species, these interactions may be considered to interfere with the freedom or availability of the ionic species to conduct charge. Furthermore, for the GLN and ADN containing mixtures, which show smaller deviations away from the Walden behavior of the neat $[Pyrr_{14}][TFSI]$ IL, no significant excess volumetric changes were observed. These observations also hold true across the wide range of compositions (i.e., from $x[Pyrr_{14}][TFSI] = 1$ to 0.1) as

highlighted in the Walden plot given as a function of formulation for the three studied binary mixtures in Figure S16.

**3.6. Electrochemical Windows.** One of the most attractive features of ILs for use as electrolytes for EDLCs is the wide electrochemical stability windows typically observed. Defined by the anodic and cathodic potentials for the onset of oxidative and reductive decomposition of the IL, respectively, this property defines the possible operative voltage range of an electrolyte for a given application. As highlighted by the equations $E = 0.5CV^2$ and $P = V^2/(4R)$ (discussed in the Introductory section), increasing the electrochemical stability and, in turn, the operative voltage of the EDLC can have significant positive impact on the energy and power capabilities of the electrolyte. However, as previously discussed, ILs are typically viscous liquids and exhibit moderate to low conductivity in their pure forms. In turn, any benefits gained through higher electrochemical stability may be negated by higher internal resistances within the device. This understanding underpins the rationale behind the current work and, while it has been shown thus far that formulation of binary mixtures using the nitrile solvents can improve transport properties of the electrolyte, it is important to assess the effects of the different solvents on the electrochemical stability formulated electrolytes.

The electrochemical windows of the $\sigma_{max}$ formulations of the BTN and ADN-containing mixtures and the neat [Pyrr$_{14}$]-[TFSI] IL were measured using cyclic voltammetry (CV) at a glassy carbon working electrode at a temperature of $305 \pm 1$ K inside an Ar-filled glovebox. The resulting electrochemical windows are shown in Figure 7. As described in the
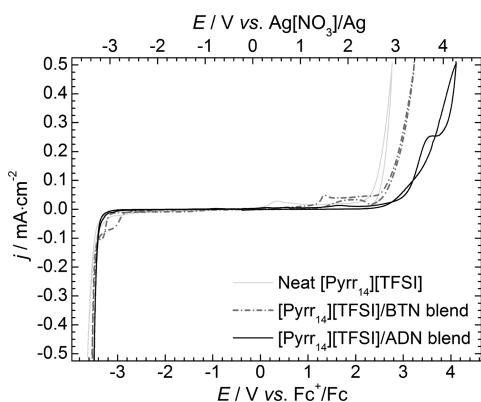


**Figure 7.** Electrochemical windows of neat [Pyrr$_{14}$][TFSI] (light-gray solid line) and the $\sigma_{max}$ compositions of the binary mixtures containing butyronitrile (gray dash-dot line) and adiponitrile (black solid line) at a glassy carbon working electrode. A scan rate of 2 mV·s$^{-1}$ was utilized and the potential of the working electrode is given vs a Ag[NO$_3$]/Ag reference electrode (top Y-axis) and normalized vs an internal reference potential of the ferrocene redox couple (bottom Y-axis).

experimental section, a scan rate of 2 mV·s$^{-1}$ was used in all cases and the counter and reference electrodes used were a platinum wire coil and a Ag[OTf]/Ag reference electrode. The reference potentials were normalized versus the formal redox potential of the reversible ferrocene oxidation couple (measured after completion of the electrochemical window measurements). The three CVs show two primary current responses associated with reductive decomposition in the cathodic region (ca. (−3.6 to −3.4) V vs Fc$^+$/Fc) and oxidative decomposition in the anodic region ((+2.4 to +3.5) V vs Fc$^+$/

Fc). In the cathodic potential region, the CVs show very little difference between the potential of reductive decomposition, indicating that the solvents do not negatively impede the reductive stability of the mixture relative to the pure IL. However, a small negative current response is observed in the BTN-containing mixture (gray dash-dot line) before the onset of massive electrolyte decomposition (ca. −3.2 V vs Fc$^+$/Fc). Since the solvents were used as received without any purification, it is quite likely this feature is the result of introduction of trace impurities from the solvent.

More variation is observed in the anodic potential region when comparing the neat IL with the two binary mixtures. Primarily, when comparing the most significant positive current responses associated with massive electrolyte decomposition, it can be seen that the presence of the BTN and ADN solvents appears to improve the oxidative stability (and the magnitude of the electrochemical window) of the resulting mixtures. Using an arbitrary cutoff current of 0.1 mA·cm$^{-2}$, the oxidative limits of the neat IL, the BTN, and ADN mixtures are found to be +2.44 V vs Fc$^+$/Fc, + 2.70 V vs Fc$^+$/Fc, and +3.21 V vs Fc$^+$/Fc, respectively. Consequently, the magnitude of the electrochemical window (i.e., the difference between anodic and cathodic potential limits) for the neat IL, the BTN, and ADN mixtures at the glassy carbon working electrode at $305 \pm 1$ K are ca. 5.8, 6.1, and 6.5 V, respectively.

Obviously, in both the binary mixtures the concentration of the ionic species at the electrode/electrolyte is significantly lower than that of the neat IL sample. However, additional interactions between IL and solvent which may help to stabilize the ionic species (most likely the anion) toward electrochemical oxidation must also be present. Additionally, small positive current responses are observed prior to the onset of electrolyte oxidative decomposition in the BTN-containing binary mixture. As indicated for the small peak observed in the negative region, it is very likely these observations are the result of oxidation of trace level impurities from the solvent. If this is correct, these additional processes could be effectively negated by careful purification of the solvent by an appropriate method of distillation.

In practical terms, the total usable voltage of an electrolyte in an EDLC device is highly dependent on the electrode material, for example at high surface area activated carbon materials with many different surface functional groups are present at the electrolyte/electrode interface. Indeed at these types of electrodes, the neat IL, [Pyrr$_{14}$][TFSI], can be utilized with an operative voltage 3.5 V,[8] compared to the 5.8 V stability window observed at the inert, low surface area, highly conductive glassy carbon electrode. Additionally, operative temperature ranges are determined by the chosen electrolyte materials of an EDLC, and usable temperature ranges of (223−373) K have been reported for IL-based electrolytes.[74] On the basis of the thermal investigations of these mixture, the operative temperature range could extend far into the subambient range and, while usable voltages in EDLCs would be expected to reduce somewhat at higher temperatures,[74] investigation of the electrochemical stability of the IL/nitrile blend electrolytes as a function of the temperature would be beneficial.

## 4. CONCLUSIONS

We have reported on the volumetric, transport, and thermal properties of binary mixtures of 1-butyl-1-methylpyrrolidinium bis{(trifluoromethyl)sulfonyl}imide ionic liquid with three

aliphatic nitrile molecular solvents as possible electrolytes for EDLC application. Thermal property data clearly showed the potential of increased liquid temperature ranges of the pure IL when mixed with BTN or ADN, opening the possibility of studying EDLC operation with selected electrolyte compositions under reduced temperatures. Investigations into the excess volumetric properties of these mixtures revealed significant negative deviations from, so-called, ideal mixing in the case of the BTN containing solvent. This is likely the result of strong interactions between the nitrile solvent and IL or improved packing of the liquid structure. However, a quasi-ideal behavior has been observed when this IL is mixed with both ADN and GLN. These observations were further supported by calculations of the excess Gibbs energies of activation of viscous flow for the binary mixtures.

As expected, measurements of viscosity of the mixtures showed the addition of these molecular solvents enables the important reduction in viscosity relative to the pure IL. Importantly, this has been shown to equate to a promotion in the electrolytic conductivity of the mixture to a certain composition, notably the $\sigma_{max}$ formulations. These properties are of very important for high power capabilities of a given electrolyte for EDLCs. Indeed, the BTN-containing mixtures exhibit a conductivity of ca. 18 mS·cm$^{-1}$ at 298 K, exceeding that of the state-of-the-art electrolyte based on a propylene carbonate solvent with 1 mol·dm$^{-3}$ tetraethylammonium tetrafluoroborate (13 mS·cm$^{-1}$ at 298 K). Nevertheless, the low volatility of the higher viscosity dinitrile solvents is of vital importance in terms of the safety of such electrolytes. Furthermore, the good electrochemical stability of this IL was found to be uninhibited by the nitrile molecular solvents at the $\sigma_{max}$ formulations at a glassy carbon electrode.

## ■ ASSOCIATED CONTENT

### ⓢ Supporting Information

The Supporting Information is available free of charge on the ACS Publications website at DOI: 10.1021/acs.jced.6b00718. Additional supporting data are openly available on Queen's University Research Portal: http://pure.qub.ac.uk/portal/en/datasets/search.html.

> NMR spectra of IL and intermediate; DSC thermograms of the IL/BTN and IL/ADN mixtures; density of the three binary mixtures as functions of the sample temperature and the linear fitting coefficients of the density−temperature relationship; calculated values for the $V_m^E$ of the binary mixtures and coefficients of the Redlich−Kister correlation of $V_m^E$ data for IL/GLN and IL/ADN mixtures; VTF and Arrhenius parameters for the correlation of the temperature dependence of viscosities; calculated values for $\Delta\eta$ and $\Delta G^{E*}$, and the respective coefficients of the Redlich−Kister correlation, for all three IL/nitrile binary mixtures; raw conductivity data, and the respective VTF parameters, for the $\sigma_{max}$ formulations of the three binary mixtures; percentage deviations of the experimental density, viscosity, and conductivity from literature values for the neat components; Walden plot of the three binary mixtures given as a function of formulation (PDF)

## ■ AUTHOR INFORMATION

### Corresponding Authors
*E-mail: aneale01@qub.ac.uk.

*E-mail: johan.jacquemin@qub.ac.uk; jj@univ-tours.fr

### ORCID ⓘ
Alex R. Neale: 0000-0001-7675-5432
Christopher Hardacre: 0000-0001-7256-6765

### Present Addresses
∥(1) Institute for Technical Chemistry and Environmental Chemistry and (2) Center for Energy and Environmental Chemistry, Friedrich-Schiller-University Jena, Philosophenweg 7a, 07743 Jena, Germany.
#School of Chemical Engineering and Analytical Science, University of Manchester, Manchester, M13 9PL, United Kingdom
ΩUniversité François Rabelais, Laboratoire PCM2E, Parc de Grandmont 37200 Tours, France

### Notes
The authors declare no competing financial interest.

## ■ REFERENCES

(1) Miller, J. R.; Burke, A. F. Electrochemical Capacitors: Challenges and Opportunities for Real-World Applications. *Electrochem. Soc. Interface* **2008**, *17*, 53−57.

(2) Wang, G.; Zhang, L.; Zhang, J. A Review of Electrode Materials for Electrochemical Supercapacitors. *Chem. Soc. Rev.* **2012**, *41*, 797−828.

(3) Béguin, F.; Presser, V.; Balducci, A.; Frackowiak, E. Carbons and Electrolytes for Advanced Supercapacitors. *Adv. Mater. (Weinheim, Ger.)* **2014**, *26*, 2219−2251.

(4) Korenblit, Y.; Rose, M.; Kockrick, E.; Borchardt, L.; Kvit, A.; Kaskel, S.; Yushin, G. High-Rate Electrochemical Capacitors Based on Ordered Mesoporous Silicon Carbide-Derived Carbon. *ACS Nano* **2010**, *4*, 1337−1344.

(5) Chmiola, J.; Yushin, G.; Gogotsi, Y.; Portet, C.; Simon, P.; Taberna, P. L. Anomalous Increase in Carbon Capacitance at Pore Sizes Less Than 1 Nanometer. *Science* **2006**, *313*, 1760−1763.

(6) Tao, Y.; Xie, X.; Lv, W.; Tang, D.-M.; Kong, D.; Huang, Z.; Nishihara, H.; Ishii, T.; Li, B.; Golberg, D.; Kang, F.; Kyotani, T.; Yang, Q.-H. Towards Ultrahigh Volumetric Capacitance: Graphene Derived Highly Dense but Porous Carbons for Supercapacitors. *Sci. Rep.* **2013**, *3*, 2975.

(7) Cheng, Q.; Tang, J.; Ma, J.; Zhang, H.; Shinya, N.; Qin, L.-C. Graphene and Carbon Nanotube Composite Electrodes for Supercapacitors with Ultra-High Energy Density. *Phys. Chem. Chem. Phys.* **2011**, *13*, 17615−17624.

(8) Balducci, A.; Dugas, R.; Taberna, P. L.; Simon, P.; Plée, D.; Mastragostino, M.; Passerini, S. High Temperature Carbon−Carbon Supercapacitor Using Ionic Liquid as Electrolyte. *J. Power Sources* **2007**, *165*, 922−927.

(9) Ruiz, V.; Huynh, T.; Sivakkumar, S. R.; Pandolfo, A. G. Ionic Liquid-Solvent Mixtures as Supercapacitor Electrolytes for Extreme Temperature Operation. *RSC Adv.* **2012**, *2*, 5591−5598.

(10) Coadou, E.; Timperman, L.; Jacquemin, J.; Galiano, H.; Hardacre, C.; Anouti, M. Comparative Study on Performances of Trimethyl-Sulfonium and Trimethyl-Ammonium Based Ionic Liquids in Molecular Solvents as Electrolyte for Electrochemical Double Layer Capacitors. *J. Phys. Chem. C* **2013**, *117*, 10315−10325.

(11) Ghamouss, F.; Brugère, A.; Jacquemin, J. Physicochemical Investigation of Adiponitrile-Based Electrolytes for Electrical Double Layer Capacitor. *J. Phys. Chem. C* **2014**, *118*, 14107−14123.

(12) Pohlmann, S.; Olyschläger, T.; Goodrich, P.; Vicente, J. A.; Jacquemin, J.; Balducci, A. Mixtures of Azepanium Based Ionic Liquids and Propylene Carbonate as High Voltage Electrolytes for Supercapacitors. *Electrochim. Acta* **2015**, *153*, 426−432.

(13) Arbizzani, C.; Biso, M.; Cericola, D.; Lazzari, M.; Soavi, F.; Mastragostino, M. Safe, High-Energy Supercapacitors Based on Solvent-Free Ionic Liquid Electrolytes. *J. Power Sources* **2008**, *185*, 1575−1579.

(14) Brandt, A.; Isken, P.; Lex-Balducci, A.; Balducci, A. Adiponitrile-Based Electrochemical Double Layer Capacitor. *J. Power Sources* **2012**, *204*, 213−219.

(15) Burke, A.; Miller, M. The Power Capability of Ultracapacitors and Lithium Batteries for Electric and Hybrid Vehicle Applications. *J. Power Sources* **2011**, *196*, 514−522.

(16) Ue, M. Chemical Capacitors and Quaternary Ammonium Salts. *Electrochemistry* **2007**, *75*, 565−572.

(17) Abdallah, T.; Lemordant, D.; Claude-Montigny, B. Are Room Temperature Ionic Liquids Able to Improve the Safety of Supercapacitors Organic Electrolytes without Degrading the Performances? *J. Power Sources* **2012**, *201*, 353−359.

(18) Wolff, C.; Jeong, S.; Paillard, E.; Balducci, A.; Passerini, S. High Power, Solvent-Free Electrochemical Double Layer Capacitors Based on Pyrrolidinium Dicyanamide Ionic Liquids. *J. Power Sources* **2015**, *293*, 65−70.

(19) Rennie, A. J. R.; Martins, V. L.; Torresi, R. M.; Hall, P. J. Ionic Liquids Containing Sulfonium Cations as Electrolytes for Electrochemical Double Layer Capacitors. *J. Phys. Chem. C* **2015**, *119*, 23865−23874.

(20) Kühnel, R. S.; Böckenfeld, N.; Passerini, S.; Winter, M.; Balducci, A. Mixtures of Ionic Liquid and Organic Carbonate as Electrolyte with Improved Safety and Performance for Rechargeable Lithium Batteries. *Electrochim. Acta* **2011**, *56*, 4092−4099.

(21) Nádherná, M.; Reiter, J.; Moškon, J.; Dominko, R. Lithium Bis(Fluorosulfonyl)Imide−Pyr14tfsi Ionic Liquid Electrolyte Compatible with Graphite. *J. Power Sources* **2011**, *196*, 7700−7706.

(22) Yang, B.; Li, C.; Zhou, J.; Liu, J.; Zhang, Q. Pyrrolidinium-Based Ionic Liquid Electrolyte with Organic Additive and Litfsi for High-Safety Lithium-Ion Batteries. *Electrochim. Acta* **2014**, *148*, 39−45.

(23) Ding, C.; Nohira, T.; Hagiwara, R.; Matsumoto, K.; Okamoto, Y.; Fukunaga, A.; Sakai, S.; Nitta, K.; Inazawa, S. Na[Fsa]-[C3c1pyrr][Fsa] Ionic Liquids as Electrolytes for Sodium Secondary Batteries: Effects of Na Ion Concentration and Operation Temperature. *J. Power Sources* **2014**, *269*, 124−128.

(24) Wongittharom, N.; Lee, T.-C.; Wang, C.-H.; Wang, Y.-C.; Chang, J.-K. Electrochemical Performance of Na/Nafepo4 Sodium-Ion Batteries with Ionic Liquid Electrolytes. *J. Mater. Chem. A* **2014**, *2*, 5655−5661.

(25) Lewandowski, A.; Olejniczak, A.; Galinski, M.; Stepniak, I. Performance of Carbon−Carbon Supercapacitors Based on Organic, Aqueous and Ionic Liquid Electrolytes. *J. Power Sources* **2010**, *195*, 5814−5819.

(26) Krause, A.; Balducci, A. High Voltage Electrochemical Double Layer Capacitor Containing Mixtures of Ionic Liquids and Organic Carbonate as Electrolytes. *Electrochem. Commun.* **2011**, *13*, 814−817.

(27) Brandt, A.; Pohlmann, S.; Varzi, A.; Balducci, A.; Passerini, S. Ionic Liquids in Supercapacitors. *MRS Bull.* **2013**, *38*, 554−559.

(28) Schütter, C.; Neale, A. R.; Wilde, P.; Goodrich, P.; Hardacre, C.; Passerini, S.; Jacquemin, J.; Balducci, A. The Use of Binary Mixtures of 1-Butyl-1-Methylpyrrolidinium Bis{(Trifluoromethyl)Sulfonyl}Imide and Aliphatic Nitrile Solvents as Electrolyte for Supercapacitors. *Electrochim. Acta* **2016**, *220*, 146−155.

(29) Phibbs, M. K. The Properties of Nitrile Binary Systems and Their Relation to Polyacrylonitrile Solubility. *J. Phys. Chem.* **1955**, *59*, 346−354.

(30) Henderson, W. A.; Passerini, S. Phase Behavior of Ionic Liquid−Lix Mixtures: Pyrrolidinium Cations and Tfsi- Anions. *Chem. Mater.* **2004**, *16*, 2881−2885.

(31) Martinelli, A.; Matic, A.; Jacobsson, P.; Börjesson, L.; Fernicola, A.; Scrosati, B. Phase Behavior and Ionic Conductivity in Lithium Bis(Trifluoromethanesulfonyl)Imide-Doped Ionic Liquids of the Pyrrolidinium Cation and Bis(Trifluoromethanesulfonyl)Imide Anion. *J. Phys. Chem. B* **2009**, *113*, 11247−11251.

(32) MacFarlane, D. R.; Meakin, P.; Sun, J.; Amini, N.; Forsyth, M. Pyrrolidinium Imides: A New Family of Molten Salts and Conductive Plastic Crystal Phases. *J. Phys. Chem. B* **1999**, *103*, 4164−4170.

(33) Kunze, M.; Jeong, S.; Paillard, E.; Winter, M.; Passerini, S. Melting Behavior of Pyrrolidinium-Based Ionic Liquids and Their Binary Mixtures. *J. Phys. Chem. C* **2010**, *114*, 12364−12369.

(34) Vitucci, F. M.; Manzo, D.; Navarra, M. A.; Palumbo, O.; Trequattrini, F.; Panero, S.; Bruni, P.; Croce, F.; Paolone, A. Low-Temperature Phase Transitions of 1-Butyl-1-Methylpyrrolidinium Bis(Trifluoromethanesulfonyl)Imide Swelling a Polyvinylidenefluoride Electrospun Membrane. *J. Phys. Chem. C* **2014**, *118*, 5749−5755.

(35) Clough, M. T.; Crick, C. R.; Grasvik, J.; Hunt, P. A.; Niedermeyer, H.; Welton, T.; Whitaker, O. P.; Physicochemical, A. Investigation of Ionic Liquid Mixtures. *Chem. Sci.* **2015**, *6*, 1101−1114.

(36) Michnick, R. B.; Sadoway, D. R. Phase Diagram of Butyronitrile−Chloroethane Determined by Differential Thermal Analysis. *J. Phys. Chem.* **1996**, *100*, 19628−19631.

(37) Vranes, M.; Dozic, S.; Djeric, V.; Gadzuric, S. Physicochemical Characterization of 1-Butyl-3-Methylimidazolium and 1-Butyl-1-Methylpyrrolidinium Bis(Trifluoromethylsulfonyl)Imide. *J. Chem. Eng. Data* **2012**, *57*, 1072−1077.

(38) Pereiro, A. B.; Veiga, H. I. M.; Esperança, J. M. S. S.; Rodríguez, A. Effect of Temperature on the Physical Properties of Two Ionic Liquids. *J. Chem. Thermodyn.* **2009**, *41*, 1419−1423.

(39) Gardas, R. L.; Costa, H. F.; Freire, M. G.; Carvalho, P. J.; Marrucho, I. M.; Fonseca, I. M. A.; Ferreira, A. G. M.; Coutinho, J. A. P. Densities and Derived Thermodynamic Properties of Imidazolium-, Pyridinium-, Pyrrolidinium-, and Piperidinium-Based Ionic Liquids. *J. Chem. Eng. Data* **2008**, *53*, 805−811.

(40) Gaciño, F. M.; Regueira, T.; Lugo, L.; Comuñas, M. J. P.; Fernández, J. Influence of Molecular Structure on Densities and Viscosities of Several Ionic Liquids. *J. Chem. Eng. Data* **2011**, *56*, 4984−4999.

(41) Jacquemin, J.; Nancarrow, P.; Rooney, D. W.; Costa Gomes, M. F.; Husson, P.; Majer, V.; Pádua, A. A. H.; Hardacre, C. Prediction of Ionic Liquid Properties. Ii. Volumetric Properties as a Function of Temperature and Pressure. *J. Chem. Eng. Data* **2008**, *53*, 2133−2143.

(42) Harris, K. R.; Woolf, L. A.; Kanakubo, M.; Rüther, T. Transport Properties of N-Butyl-N-Methylpyrrolidinium Bis-(Trifluoromethylsulfonyl)Amide. *J. Chem. Eng. Data* **2011**, *56*, 4672−4685.

(43) Tokuda, H.; Tsuzuki, S.; Susan, M. A. B. H.; Hayamizu, K.; Watanabe, M. How Ionic Are Room-Temperature Ionic Liquids? An Indicator of the Physicochemical Properties. *J. Phys. Chem. B* **2006**, *110*, 19593−19600.

(44) Vraneš, M.; Tot, A.; Papović, S.; Zec, N.; Dožić, S.; Gadžurić, S. Ideal and Non-Ideal Behaviour of {1-Butyl-1-Methylpyrrolydinium Bis(Trifluoromethylsulfonyl)Imide + Γ-Butyrolactone} Binary Mixtures. *J. Chem. Thermodyn.* **2015**, *81*, 66−76.

(45) Dong, Q.; Muzny, C. D.; Kazakov, A.; Diky, V.; Magee, J. W.; Widegren, J. A.; Chirico, R. D.; Marsh, K. N.; Frenkel, M. Ilthermo: A Free-Access Web Database for Thermodynamic Properties of Ionic Liquids. *J. Chem. Eng. Data* **2007**, *52*, 1151−1159.

(46) Grzeskowiak, R.; Jeffery, G. H.; Vogel, A. I. 921. Physical Properties and Chemical Constitution. Part Xxxi. Polymethylene Dichlorides, Dibromides, Di-Iodides, and Dicyanides. *J. Chem. Soc.* **1960**, 4728−4731.

(47) Woodman, A. L.; Murbach, W. J.; Kaufman, M. H. Vapor Pressure and Viscosity Relationships for a Homologous Series of A,I-Dinitriles. *J. Phys. Chem.* **1960**, *64*, 658−660.

(48) Haijun, W.; Mingzhi, C.; Guokang, Z. Excess Volumes of (an Aliphatic Dinitrile + an Aromatic Hydrocarbon) at the Temperature 298.15 K. *J. Chem. Thermodyn.* **1994**, *26*, 913−918.

(49) Sears, P. G.; Caruso, J. A.; Popov, A. I. Conductances of Some Uni-Univalent Electrolytes in Adiponitrile at 25.Degree. *J. Phys. Chem.* **1967**, *71*, 905−909.

(50) Oswal, S. L.; Patel, N. B. Speed of Sound, Isentropic Compressibility, Viscosity, and Excess Volume of Binary Mixtures. 1. Alkanenitriles with Alkyl Acetates. *J. Chem. Eng. Data* **1995**, *40*, 840−844.

(51) Letcher, T. M.; Naicker, P. K. Excess Molar Enthalpies and Excess Molar Volumes of (an Alkanol + a Nitrile Compound) Att= 298.15 K Andp= 0.1 MPa. *J. Chem. Thermodyn.* **2001**, *33*, 1035−1047.

(52) Gill, D. S.; Rana, D. S.; Jauhar, S. P. Compressibility Studies of Some Copper(I), Silver(I), and Tetrabutylammonium Salts in Acetonitrile + Adiponitrile Binary Mixtures. *J. Chem. Eng. Data* **2010**, *55*, 2066−2071.

(53) Jeffery, G. H.; Vogel, A. I. 134. Physical Properties and Chemical Constitution. Part Xvii. Acetylenic Compounds and Cyanides. *J. Chem. Soc.* **1948**, 674−683.

(54) Rajagopal, K.; Chenthilnath, S.; Nain, A. K. Physicochemical Studies of Molecular Interactions in Binary Mixtures of Toluene with Some Aliphatic Nitriles at Different Temperatures. *J. Mol. Liq.* **2010**, *151*, 23−29.

(55) Mehta, S. K.; Sharma, A. K. Effect of Cn Group on Isentropic Compressibility and Volumetric Parameters of Mixtures of Γ-Butyrolactam (N = 5) and Nitriles. *Fluid Phase Equilib.* **2003**, *205*, 37−51.

(56) Martínez, S.; Garriga, R.; Pérez, P.; Gracia, M. Densities and Viscosities of Binary Mixtures of Butanenitrile with Butanol Isomers at Several Temperatures. *J. Chem. Eng. Data* **2000**, *45*, 1182−1188.

(57) López-Lázaro, J. d. l. S.; Iglesias-Silva, G. A.; Estrada-Baltazar, A.; Barajas-Fernández, J. Density and Surface Tension of Binary Mixtures of 2,2,4-Trimethylpentane + N-Heptane, 2,2,4-Trimethylpentane + N-Octane, Ethyl Acetate + Benzene, and Butanenitrile + Benzene from (293.15 to 323.15) K. *J. Chem. Eng. Data* **2015**, *60*, 1823−1834.

(58) Jannelli, L.; Pansini, M.; Jalenti, R. Partial Molar Volumes of C2-C5 Normal and Branched Nitriles in Sulfolane Solutions at 30.Degree.C. *J. Chem. Eng. Data* **1984**, *29*, 263−266.

(59) Domańska, U.; Marciniak, M. Experimental (Solid + Liquid) and (Liquid + Liquid) Equilibria and Excess Molar Volume of Alkanol + Acetonitrile, Propanenitrile, and Butanenitrile Mixtures. *J. Chem. Eng. Data* **2005**, *50*, 2035−2044.

(60) Friend, J. N.; Hargreaves, W. D. Lxxi. Viscosities and Rheochors of Aldehydes, Nitrites and of Secondary and Tertiary Amines. *London, Edinburgh, and Dublin Philosophical Magazine and Journal of Science* **1944**, *35*, 619−631.

(61) Abu-Lebdeh, Y.; Davidson, I. New Electrolytes Based on Glutaronitrile for High Energy/Power Li-Ion Batteries. *J. Power Sources* **2009**, *189*, 576−579.

(62) Kapadi, U. R.; Hundiwale, D. G.; Patil, N. B.; Lande, M. K.; Patil, P. R. Studies of Viscosity and Excess Molar Volume of Binary Mixtures of Propane-1,2 Diol with Water at Various Temperatures. *Fluid Phase Equilib.* **2001**, *192*, 63−70.

(63) Anouti, M.; Jacquemin, J.; Lemordant, D. Volumetric Properties, Viscosities, and Isobaric Heat Capacities of Imidazolium Octanoate Protic Ionic Liquid in Molecular Solvents. *J. Chem. Eng. Data* **2010**, *55*, 5719−5728.

(64) Yang, X.; Song, H.; Wang, J.; Zou, W. Temperature and Composition Dependence of the Density, Viscosity and Refractive Index of Binary Mixtures of a Novel Gemini Ionic Liquid with Acetonitrile. *RSC Adv.* **2016**, *6*, 29172−29181.

(65) Chen, J.; Chen, L.; Xu, Y. Properties of Pure 1,1,3,3-Tetramethylguanidine Imidazole Ionic Liquid and Its Binary Mixtures with Alcohols at T = (293.15 to 313.15) K. *J. Chem. Thermodyn.* **2015**, *88*, 110−120.

(66) Lide, D. R. *CRC Handbook of Chemistry and Physics*, 84th ed.; CRC Press, 2003−2004.

(67) Yang, Q.; Chen, K.; He, C.; Peng, C.; Liu, H. Vapor Pressure Measurement and Correlation of Acetonitrile + 1-Butyl-3-Methyl-imidazolium Chloride, + 1-Butyl-3-Methylimidazolium Tetrafluoroborate, and + 1-Hexyl-3-Methylimidazolium Chloride. *Chin. J. Chem. Eng.* **2015**, *23*, 412−416.

(68) Zafarani-Moattar, M. T.; Shekaari, H. Application of Prigogine−Flory−Patterson Theory to Excess Molar Volume and Speed of Sound of 1-N-Butyl-3-Methylimidazolium Hexafluorophosphate or 1-N-Butyl-3-Methylimidazolium Tetrafluoroborate in Methanol and Acetonitrile. *J. Chem. Thermodyn.* **2006**, *38*, 1377−1384.

(69) Ue, M.; Ida, K.; Mori, S. Electrochemical Properties of Organic Liquid Electrolytes Based on Quaternary Onium Salts for Electrical Double-Layer Capacitors. *J. Electrochem. Soc.* **1994**, *141*, 2989−2996.

(70) Ueno, K.; Tokuda, H.; Watanabe, M. Ionicity in Ionic Liquids: Correlation with Ionic Structure and Physicochemical Properties. *Phys. Chem. Chem. Phys.* **2010**, *12*, 1649−1658.

(71) Fraser, K. J.; Izgorodina, E. I.; Forsyth, M.; Scott, J. L.; MacFarlane, D. R. Liquids Intermediate between ″Molecular″ and ″Ionic″ Liquids: Liquid Ion Pairs? *Chem. Commun.* **2007**, 3817−3819.

(72) MacFarlane, D. R.; Forsyth, M.; Izgorodina, E. I.; Abbott, A. P.; Annat, G.; Fraser, K. On the Concept of Ionicity in Ionic Liquids. *Phys. Chem. Chem. Phys.* **2009**, *11*, 4962−4967.

(73) Galiński, M.; Lewandowski, A.; Stępniak, I. Ionic Liquids as Electrolytes. *Electrochim. Acta* **2006**, *51*, 5567−5580.

(74) Lin, R.; Taberna, P.-L.; Fantini, S.; Presser, V.; Pérez, C. R.; Malbosc, F.; Rupesinghe, N. L.; Teo, K. B. K.; Gogotsi, Y.; Simon, P. Capacitive Energy Storage from − 50 to 100 °C Using an Ionic Liquid Electrolyte. *J. Phys. Chem. Lett.* **2011**, *2*, 2396−2401.